THE ASTROPHYSICAL JOURNAL SUPPLEMENT SERIES, 73:747–768, 1990 August

STRUCTURE IN SMALL MOLECULAR CLOUDS: PEDESTALS AND CLUMPING

LORIS MAGNANI
Arecibo Observatory[1]
JOHN M. CARPENTER
University of Massachusetts and Arecibo Observatory
LEO BLITZ
University of Maryland
NAMIR E. KASSIM[2]
Center for Advanced Space Sensing, Naval Research Laboratory
AND
BIMAN B. NATH
University of Maryland
Received 1989 October 16; accepted 1989 December 12

ABSTRACT

Observations of wings or pedestals in the CO($J = 1$–0) and CO($J = 2$–1) transitions from three regions in high-latitude molecular clouds are presented in order to determine the morphology and physical conditions of the gas responsible for this phenomenon. High-sensitivity spectra along 10–25 lines of sight in each region show extended ($\Delta v \sim 3$–5 km s^{-1}), low-level ($T_R^* \leq 0.5$ K) emission in addition to the typical narrow Gaussian emission from cold clumps. The pedestal profiles resemble the wings seen in CO and other molecules in low-luminosity molecular outflow regions such as B335. In the case of the bipolar outflows, the energy required to drive the outflow comes from a young stellar object; in contrast, it is virtually certain that the small molecular clouds studied in this paper do *not* contain any low-mass star formation sites.

The ^{13}CO and CO($J = 2$–1) data indicate that the pedestal emission is optically thick. Large velocity gradient and LTE analyses using CO($J = 1$–0), ^{13}CO($J = 1$–0), and CO($J = 2$–1) data indicate that the narrow-line emission is produced by cold clumps of size ~ 0.2 pc and density several times 10^3 cm^{-3}, while the pedestal emission is produced by gas with perhaps an order of magnitude less density.

Adjacent spectra often reveal a pedestal which increases in antenna temperature until it resembles a narrow Gaussian line typical of clump emission. This change in spectral shape occurs over length scales of a few hundredths of a parsec and may represent the transition region between a dense clump and its less dense outer region. Possible explanations for the phenomenon include: (1) A suggestion recently made by Keto and Lattanzio that the pedestals represent gas flowing at the interface of two colliding clouds. The observed spectra are due to a combination of bulk motion and projection effects. (2) The superposition of two clumps situated so that the line of sight traverses the central portion of one clump and the outer region of the other. A decrease in the surface filling fraction of gas in the outer regions of a clump can produce the observed low antenna temperatures of the pedestal by beam dilution.

Subject headings: interstellar: molecules — nebulae: internal motions — nebulae: structure

I. INTRODUCTION

Spectra of the CO($J = 1$–0) transition from small, quiescent molecular clouds typically show a single Gaussian emission line with a FWHM of few km s^{-1} or less at or near the cloud systemic velocity. These narrow lines are indicative of local density enhancements in the cloud loosely referred to as "clumps." Although most small, dark molecular clouds are characterized by a single narrow Gaussian line, some lines of sight clearly show separate components consisting of more than one Gaussian profile (Clark, Giguerre, and Crutcher 1977). Furthermore, emission at a lower antenna temperature ($T_A^* < 1$ K) than the narrow-line component sometimes extends on one or both sides of the Gaussian line profile. This "wing" or pedestal emission is observed in giant molecular clouds or large star-forming molecular complexes (e.g., Lada 1985) and in isolated, dark molecular clouds (Frerking and Langer 1982; Lichten 1982; Goldsmith, Langer, and Wilson 1986; Heyer *et al.* 1987; Schwartz, Gee, and Huang 1988; Armstrong and Winnewisser 1989). In virtually all instances, the pedestal emission has been attributed to gas flowing out from a dense molecular core within a clump. These outflows are thought to be driven by the wind from one or more T Tauri stars or other young stellar or protostellar objects.

[1]Arecibo Observatory is part of the National Astronomy and Ionosphere Center which is operated by Cornell University under a management agreement with the National Science Foundation.
[2]ONT–NRL Research Fellow.

Report Documentation Page

Form Approved
OMB No. 0704-0188

1. REPORT DATE	2. REPORT TYPE	3. DATES COVERED
AUG 1990		**00-00-1990 to 00-00-1990**

4. TITLE AND SUBTITLE	5a. CONTRACT NUMBER
Structure in Small Molecular Clouds: Pedestals and Clumping	5b. GRANT NUMBER
	5c. PROGRAM ELEMENT NUMBER
6. AUTHOR(S)	5d. PROJECT NUMBER
	5e. TASK NUMBER
	5f. WORK UNIT NUMBER
7. PERFORMING ORGANIZATION NAME(S) AND ADDRESS(ES) **Naval Research Laboratory,Code 7213,4555 Overlook Avenue, SW,Washington,DC,20375**	8. PERFORMING ORGANIZATION REPORT NUMBER
9. SPONSORING/MONITORING AGENCY NAME(S) AND ADDRESS(ES)	10. SPONSOR/MONITOR'S ACRONYM(S)
	11. SPONSOR/MONITOR'S REPORT NUMBER(S)

12. DISTRIBUTION/AVAILABILITY STATEMENT
Approved for public release; distribution unlimited

13. SUPPLEMENTARY NOTES

14. ABSTRACT

15. SUBJECT TERMS

16. SECURITY CLASSIFICATION OF:			17. LIMITATION OF ABSTRACT	18. NUMBER OF PAGES	19a. NAME OF RESPONSIBLE PERSON
a. REPORT	b. ABSTRACT	c. THIS PAGE			
unclassified	**unclassified**	**unclassified**		**22**	

Recently, pedestal emission or extended wings have been observed in certain small molecular clouds which almost certainly do not contain young stellar objects. The objects include the diffuse molecular cloud in front of ζ Ophiuchi (Langer, Glassgold, and Wilson 1987; hereafter LGW), some of the high-latitude molecular clouds (Blitz, Magnani, and Wandel 1988; hereafter BMW; Falgarone and Pérault 1988), some of the small molecular clouds around α Orionis (Knapp and Bowers 1988), and one of the sources in the molecular outflow survey of Levreault (1988). All of these observations consist of deep CO($J = 1$–0) [hereafter CO($J = 1$–0) and CO($J = 2$–1) will be referred to as CO(1–0) and CO(2–1), respectively] spectra of relatively nearby ($d < 400$ pc) small clouds, so that the phenomenon may be generally characteristic of small molecular clouds given sufficient angular resolution and sensitivity. Pedestal emission has also been detected throughout the Rosette giant molecular cloud by Blitz and Stark (1986), who attribute the emission to a low-density pervasive interclump medium in which denser clumps are embedded. It is not yet clear if the pedestal emission from these two different types of cloud is produced by the same mechanism or physical conditions.

In this paper we discuss CO(1–0) and CO(2–1) observations of pedestal emission from small regions in three of the high-latitude molecular clouds. Section II of the paper describes the observing procedure and data reduction. The available data include relatively low sensitivity channel maps of the pedestal regions and deep spectra along at least 10 lines of sight within each mapped region. The extent and morphology of the pedestal emission with respect to the narrow line emission indicative of the clump is discussed in § III. Unfortunately, in no instance is the pedestal phenomenon completely mapped. In § IV the line profiles are analyzed using LTE and LVG methods to determine the physical parameters of the clump and pedestal. The relationship of the pedestal emission to the clump structure of a small cloud is discussed in § V, and two models which may explain the observed profiles are presented.

II. OBSERVATIONS AND DATA REDUCTION

The data were obtained during two separate runs at the NRAO[3] 12 m telescope at Kitt Peak. The CO(1–0) observations were carried out in 1986 October and were obtained by position switching against an emission-free reference position determined from the CO(1–0) maps presented in Magnani, Blitz, and Mundy (1985, hereafter MBM).

The CO(1–0) data were obtained with a dual channel SIS receiver sensitive to orthogonal polarizations with each polarization fed into one half of a 256 channel filter bank spectrometer with a resolution of 100 kHz (0.26 km s^{-1}) per channel. Simultaneously, one polarization was fed into a 128 channel filter bank with 30 kHz (0.08 km s^{-1}) resolution per channel. The resulting velocity coverage for the 115.2712 GHz CO(1–0) transition is 33 km s^{-1} for the 100 kHz filter bank and 10 km s^{-1} for the 30 kHz filter bank. The central velocity channels of the spectrometers were set so that the narrow line emission was centered in the spectra; all velocities in this paper are with respect to the LSR.

The CO(2–1) observations were obtained in 1988 January with a dual orthogonal polarization Schottky mixer receiver with each polarization again fed into one half of a 256 channel, 100 kHz filter bank, and, simultaneously, into a 250 kHz filter bank spectrometer. The velocity resolution and velocity coverage for the 230.5380 GHz CO(2–1) transition are 0.13 and 16.6 km s^{-1} for the 100 kHz filter bank and 0.33 and 41.6 km s^{-1} for the 250 kHz filter bank.

The typical system temperature referred outside the atmosphere was ~ 700 K for the CO(1–0) data and 1300–1800 K for the CO(2–1) data. At 115 GHz the FWHM of the 12 m telescope beam is 60″ and one half of that value at 230 GHz. During the CO(2–1) run the pointing was checked several times a day using the planets Jupiter, Saturn, and Mars.

The antenna temperatures from the NRAO 12 m telescope are displayed as T_R^*, that is, the antenna temperature corrected for forward scattering and spillover (Kutner and Ulich 1981). To obtain true source radiation temperatures requires knowing the source coupling factor, η_c, ($T_R = T_R^*/\eta_c$). Because η_c is a function of the source size and the extent of the pedestals in the clouds is not known, η_c is taken to be 1 in the remainder of the paper so that $T_R^* = T_R$. This will not be correct if there is significant structure on scales smaller than the beam. Finally, the spectra were reduced by subtracting only linear baselines from the raw data.

III. EXTENT AND MORPHOLOGY OF THE PEDESTALS

The regions chosen for this study are located in clouds 16, 32, and 54 of the MBM compilation. The three particular clouds in this study have substantial molecular abundances but very low extinctions; van Dishoeck and Black (1987) have named similar objects (i.e., clouds with $1 < A_V < 5$ mag) "translucent" molecular clouds to differentiate them from the classical diffuse clouds and the dark molecular clouds. Similarly, Lada and Blitz (1988) have proposed the existence of a "CO-rich" class of diffuse molecular clouds to explain the low extinctions and high CO abundances in these objects. It is important to note that the three clouds in this study have an extinction averaged over the molecular component of the cloud of $A_V \leq 1$ mag (Magnani and de Vries 1986); these objects are thus at the low extinction range of the translucent molecular clouds and along some lines of sight they may resemble more closely diffuse molecular clouds.

The pedestals were found during high-resolution mapping of several cores in the high-latitude clouds. Because the weakest pedestals have antenna temperatures of a few tenths Kelvin, it is necessary to achieve very low rms levels to detect the features. No systematic, high-sensitivity surveys with sufficient angular resolution over an entire translucent cloud have been published to date, and even the three regions studied in this paper are not completely mapped with sufficient sensitivity. Consequently, we do not know for any of the sources the full extent of the pedestal emission.

For each of the regions, low-sensitivity CO(1–0) channel maps were produced in order to determine the relationship

[3]The National Radio Astronomy Observatory is operated by Associated Universities, Inc., under contract with the National Science Foundation.

TABLE 1

LOCATIONS OF THE CO(1–0) MAPPED REGIONS[a]

Source	α (1950)	δ (1950)	Size of Region[b]
MBM 16.....	$03^h16^m12^s$	11°18′35″	11′×8′
MBM 32.....	$09^h26^m05^s$	66°05′00″	5′×7′[c]
MBM 54.....	$23^h06^m48^s$	18°13′00″	9′×9′

[a] 60″ resolution and sampling.
[b] Dimensions are R.A. and Decl.
[c] Incompletely mapped.

of the pedestal emission to the more prominent clump emission characterized by a single, narrow-line-width Gaussian line. The centers of the mapped areas within the three high-latitude clouds are given in Table 1. Since these were the only regions studied in detail, it is difficult to estimate how common the pedestal phenomenon is in these small clouds. Most lines of sight do not show evidence for the pedestal. Moreover, averages over many lines of sight also do not show such wings frequently. The broad lines discussed here therefore appear uncommon, but how uncommon is not yet clear.

Channel maps (right ascension and declination maps at a given velocity) in the CO(1–0) transition for the three regions are presented in Figures 1–3. The channel maps for MBM 16 and MBM 32 were obtained from an earlier observing run at the NRAO 12 m telescope and are described in more detail in Magnani (1987). Figures 4 and 5 show the lines of sight of the CO(1–0) and CO(2–1) high-sensitivity scans for MBM 16 and MBM 32 superposed on the channel map with the most representative velocity of the clump emission. Because of the complex structure of MBM 54, the positions of the high-sensitivity spectra are shown in Figure 6 superposed on an integrated antenna temperature map rather than on a channel map. The morphology and extent of the pedestal and clumps for the individual studied regions are described below.

MBM 32.—The CO(1–0) channel maps in Figure 2 show two distinct clumps within the 8′×16′ mapped area. The clump which shows traces of a pedestal is the westernmost of the two clumps with the narrow-line emission extending from $v = -0.9$ to -3.0 km s^{-1}. At a distance typical of the high-latitude clouds (100 pc; MBM) the clump itself is ~ 0.1 pc×0.1 pc. Clumped structures of this size are common and have been observed in giant molecular clouds (Pérault, Falgarone, and Puget 1985; Evans, Kutner, and Mundy 1987), dark molecular cloud complexes (Schneider and Elmegreen 1979; Myers and Benson 1983), and high-latitude molecular clouds (Magnani 1987). Substructure in the clump at the telescope resolution (1′) is evident; at the cloud distance, this substructure corresponds to ~ 0.03 pc in scale. Similar condensations are noted by Falgarone and Pérault (1988), who attribute them to very small scale density enhancements which are likely to be transient phenomena in the context of the larger 0.1–0.2 pc clumps which confine them. Structure at the 0.03 pc size scales appears to be common in the high-latitude molecular clouds (Magnani 1987) and will be discussed in a future paper. Twenty-five deep CO(1–0) spectra with rms noise levels ranging from 0.04 to 0.16 K were obtained at the positions denoted by the lightly shaded circles in Figure 5, and the resulting map of the spectra is shown in Figure 7.

Three main narrow-line emission components are noticeable, one centered at $v \sim -2.8$ km s^{-1} and prominent throughout the mapped region, one centered at $v \sim -1.7$ km s^{-1} in the eastern side of the map, and one centered at $v \sim -4.2$ km s^{-1} in the western and northeastern portions of the map. At positions 2′ and 3′ east of the (0,0) position (defined to be at the intersection of the labeled ordinate and abscissa in Fig. 7) the narrow line components are blended and extend from -4.2 to -0.4 km s^{-1}.

With the exceptions of a few lines of sight [e.g., (1, −2)[4]], there are traces of the pedestal throughout the mapped region. This is confirmed by Figure 8 which shows the superposition of all 25 spectra in Figure 7 plus four additional spectra at the corners of a 10′×10′ grid centered on position (0,0). If the pedestals were not present in most of the scans, the superposition of scans not containing this emission would dilute the pedestal enough to make it indistinguishable. The pedestal emission in the sum of the scans extends from $v \sim -5.7$ to -0.2 km s^{-1}; on the blueshifted side this is well beyond the most blueshifted portion of the narrow line component at $v \sim -4$ km s^{-1}.

Throughout the map it is difficult to differentiate the pedestal emission from the narrow line components for many of the lines of sight. For instance, the sequence of spectra at 0′N extending from 0′W to 2′W shows a blueshifted pedestal and a clump at $v \sim -2.8$ km s^{-1} at position (0,0) change into what decidedly looks like emission from the main clump at -2.8 km s^{-1} and another separate clump component at $v \sim -4.2$ km s^{-1} at position (−2,0). Similarly, for the sequence at 1′N extending from 1′E to 4′E, the emission appears to be composed of one broad Gaussian line at 1′E and 2′E, two narrow lines at 3′E, and a pedestal with no superposed clump component at 4′E.

Channel maps for the high-sensitivity spectra are shown in Figure 9. The clump components at -2.8 and -1.7 km s^{-1} stand out clearly, while the component at -4.2 km s^{-1} is less noticeable and appears to extend to the northeast corner of the map. None of the components are clearly separated spatially and with a lowest contour level of 0.5 K, the pedestal emission is not fully traced.

Three position-velocity plots for this region are shown in Figures 10*a*–10*c*, and they confirm the complex nature of the pedestal emission in this part of the cloud. In a position-velocity diagram, a Gaussian line profile will show relatively linear spacing between contours except for those contours near the peak and near the base of the Gaussian. Our lowest contour in the position-velocity diagrams is in the quasi-linear regime so that a deviation from linear spacing of the lowest contours is indicative of a non-Gaussian component. The slice in right ascension along 1′N shows a wide profile from 4′E to 1′W abruptly becoming a narrow component (FWHM < 1 km s^{-1}) at position 2′W (Fig. 10*a*). For the N/S direction along the slice at 1′W, Figure 10*b* shows a clump

[4] The first component is the east/west coordinate and the second is the north/south coordinate; east and north are positive. The stepsize is 1′ and the central position, (0,0), for MBM 32 is 9^h25^m9 and 66°05.

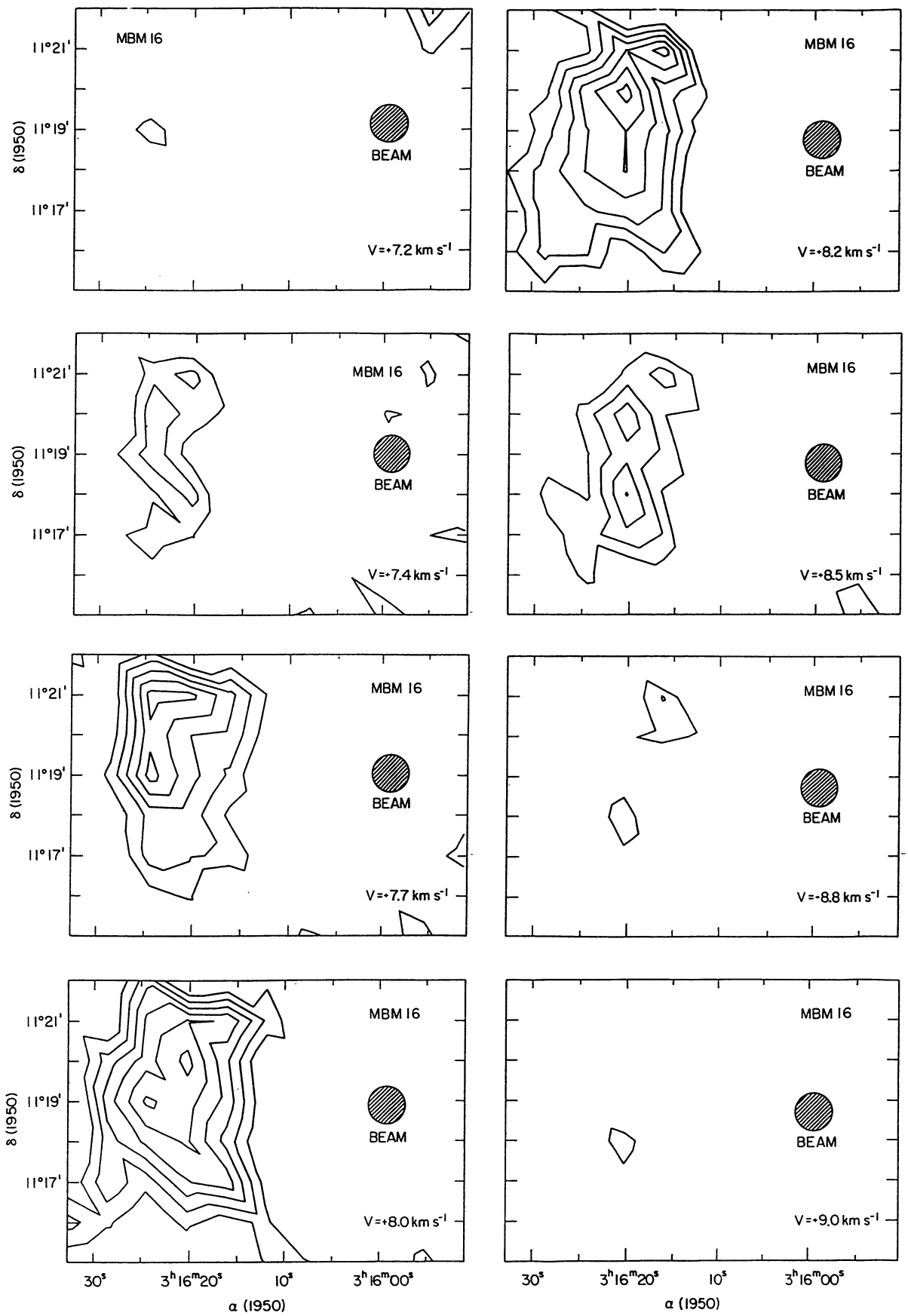

FIG. 1.—CO(1–0) channel maps of a core region in MBM 16 at full beamwidth sampling (1′). The contour levels are set at $T_R^* = 1.5$, 2.25, 3.0, 3.75, and 4.5 K with an rms noise per channel of 0.7 K. The velocity resolution is 0.26 km s^{-1}.

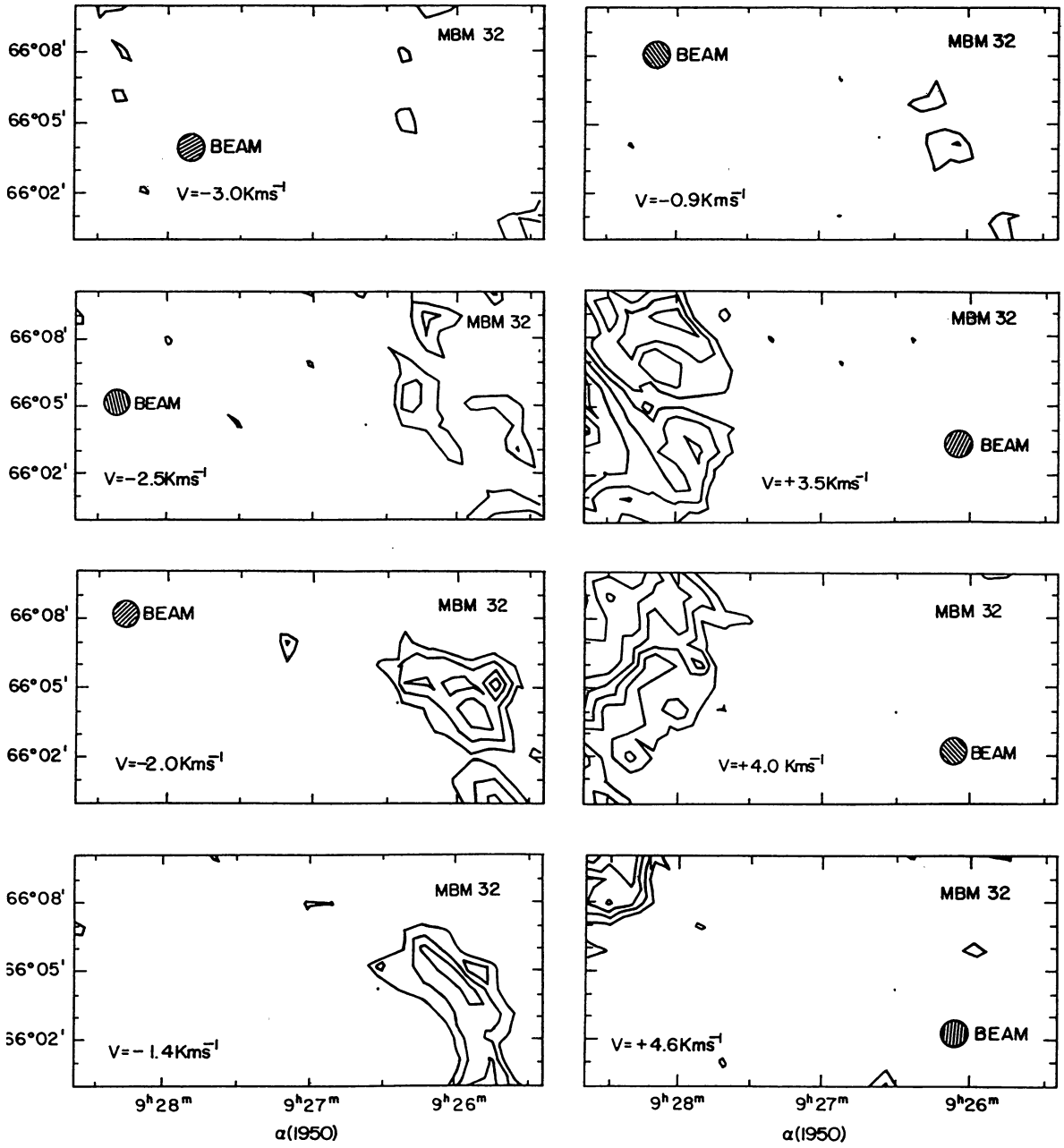

FIG. 2.—Same as Fig. 1 but for a core region in MBM 32.

with a non-Gaussian blueshifted pedestal component at locations 2′N, 0′N, and 1′S, while Figure 10*c* shows the N/S slice at 2′E and a marked non-Gaussian profile at positions 2′N, 1′S, and 2′S.

The CO(2–1) map (see Fig. 11) is oriented with position (0,0) denoted as the spectrum at the intersection of the labeled ordinate and abscissa in the figure, with 1950 coordinates $9^h25^m50^s$ and 66°05′00″. Our map is reminiscent of the high-sensitivity CO(1–0) spectra of the region around ζ Ophiuchi by LGW. However, these authors interpret their pedestal emission as composed of separate, narrow Gaussian components (see § V*b*). We call attention to the CO(2–1) spectra because they show that the pedestal emission becomes narrow Gaussian emission on a scale of 30″–60″ which at the canonical distance of the high-latitude clouds corresponds to 0.015–0.03 pc. The CO(2–1) scans also show the same type of profiles as the CO(1–0) data: For instance, a blueshifted pedestal feature at (0,0) and (0, −1) becomes a distinct narrow component clearly separate from the main clump component at positions (−2,0) and (−2, −1).

In summary, the complex interplay and transition between the pedestal and the narrow Gaussian features in MBM 32 precludes associating a pedestal feature along a particular line of sight with a nearby clump, so it is difficult to establish what is the relationship between the two types of features. However, it is clear that the pedestal can change into a

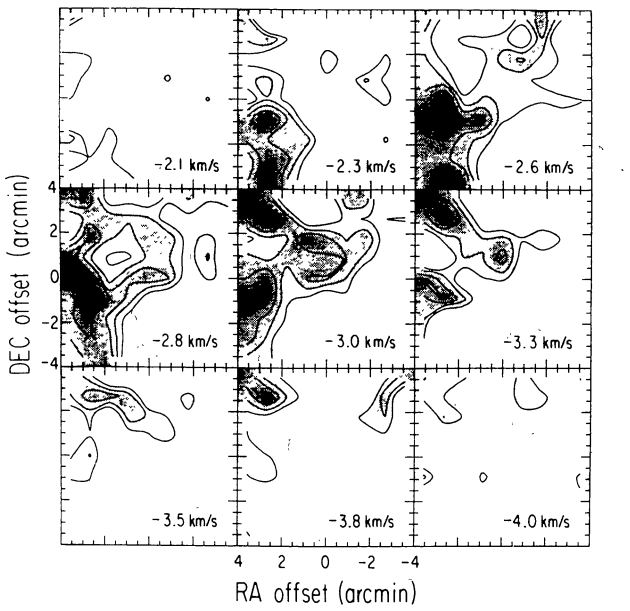

FIG. 3.—CO(1–0) channel maps for a core region in MBM 54 at full beamwidth sampling (1′). The contour levels are set at 2.5 K and at succeeding 1 K intervals. The velocity resolution is 0.08 km s^{-1}, the rms noise is ~0.8 K, and the central map position is at $23^h06^m48^s.0$ and 18°13′00″.

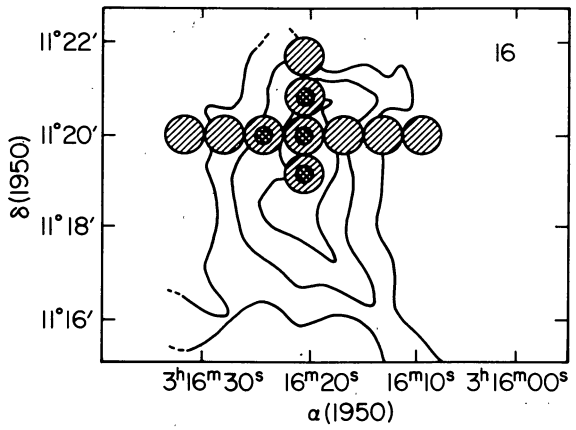

FIG. 4.—Channel map of the MBM 16 region at $v = 8.0$ km s^{-1}; same as in Fig. 1, but with contours at 1.5, 3.0, and 4.5 K. The larger stippled circles indicate the telescope beam size at 115 GHz and the locations of the high-sensitivity CO(1–0) spectra which are individually shown in Fig. 15; the smaller cross-hatched circles indicate the CO(2–1) beam size at 230 GHz and the locations of the high-sensitivity spectra which are individually shown in Fig. 16.

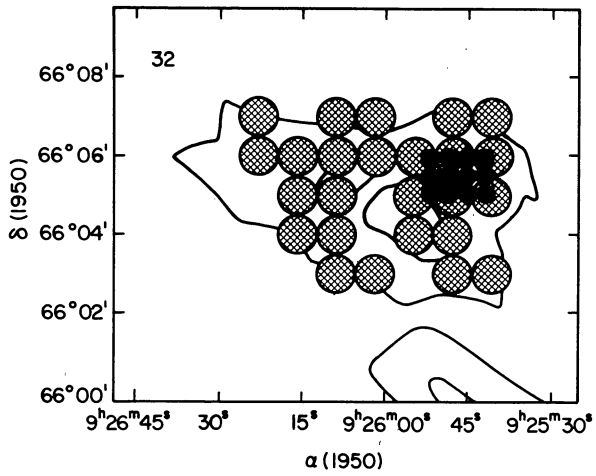

FIG. 5.—Channel map of the MBM 32 region at $v = -2.0$ km s^{-1}; same as in Fig. 4, but with contours at 1.5 and 3.0 K. The larger cross-hatched circles show the positions of the high sensitivity CO(1–0) spectra which are shown individually in Fig. 7 and the smaller, black circles show the CO(2–1) positions which are individually shown in Fig. 11.

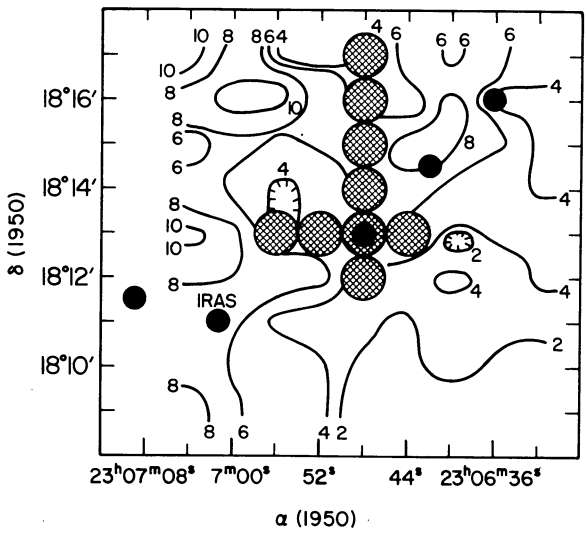

FIG. 6.—CO(1–0) integrated antenna temperature ($\int T_R^* dv$) of the core region in MBM 54. The contour levels are set at 2, 4, 6, 8, and 10 K km s^{-1} with the appropriate levels noted at the map edges. The larger cross-hatched circles indicate the telescope beam size and locations of the CO(1–0) high-sensitivity spectra (shown in Fig. 12) and the smaller, black circles indicate the beam size and locations of the CO(2–1) high-sensitivity observations (shown in Fig. 14). The small shaded circle marked "IRAS" coincides with the position of the only *IRAS* point source within the confines of the field (see § III).

distinct clump on a spatial scale of a few hundredths of a parsec.

MBM 54.—The 9′×9′ mapped region for MBM 54 is more complex than in the previous instance. At least four separate clumps are identifiable in the channel maps shown in Figure 3. The integrated antenna temperature map in Figure 6 shows a northeast-southwest gradient of emission with virtually the entire region showing $\int T_R^* dv > 2$ K km s^{-1}.

Figure 12 shows the CO(1–0) high-sensitivity map for the region in MBM 54. As in the case of MBM 32, the pedestal appears in virtually all of the spectra; however, for the northernmost spectra it increases in antenna temperature until at positions (0,3) and (0,4) it resembles a distinct narrow Gaussian profile. Close scrutiny of the spectra at position (0,3) and (0,4) reveals traces of a blueshifted pedestal, and position (0,4) shows also redshifted pedestal emission so that the pedestal does not fully disappear even as the second clump emerges. The CO(1–0) high-sensitivity spectra are mostly situated away from areas in the map with

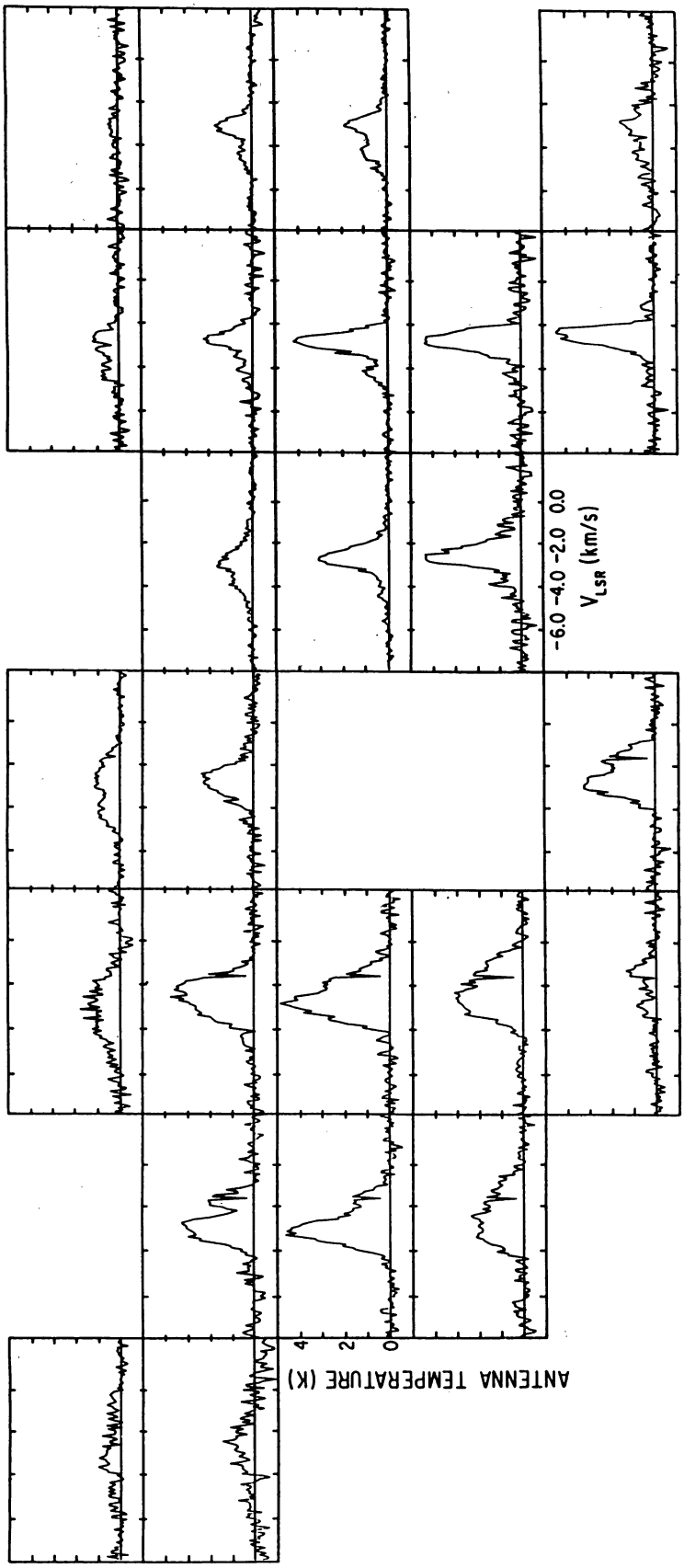

FIG. 7.—CO(1–0) high-sensitivity map at the positions in MBM 32 shown in Fig. 5. The rms noise per channel varies from 0.04 to 0.16 K and the velocity resolution is 0.08 km s^{-1}. The dip often present in the spectra at $v \sim -1.7$ km s^{-1} is due to a bad channel. Position (0,0) at $9^h25^m5\overset{s}{.}5$ and 66°05′00″ is defined to be the spectrum at the intersection of the labeled ordinate and abscissa. The spectra are a beamwidth apart (1′), corresponding to 0.03 pc at the distance of the cloud.

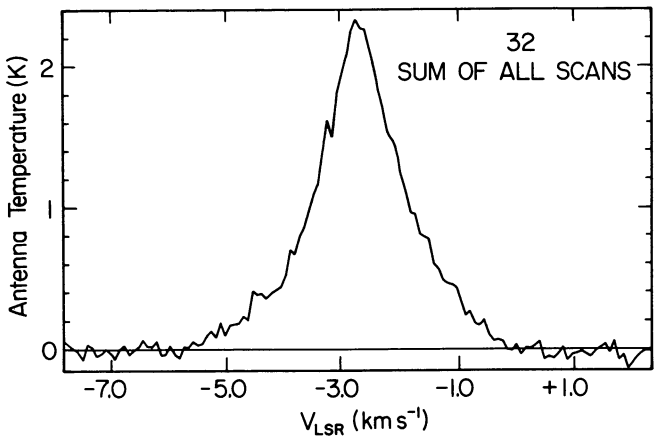

FIG. 8.—Sum of all the CO(1–0) scans in Fig. 7 plus 4 other scans at the corners of a 10′ grid centered on the (0,0) position. The rms noise of the spectrum is ~ 0.05 K and the velocity resolution is 0.08 km s^{-1}.

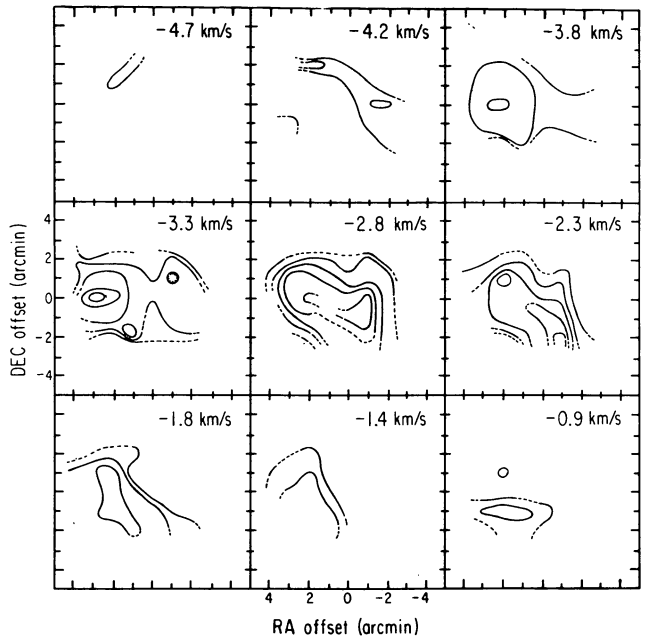

FIG. 9.—Channel maps of the high-sensitivity spectra from Fig. 7. The contours are at 0.5, 1, and 2 K and at succeeding 1 K intervals. The velocity of each individual map is noted in the top right-hand corner of each frame.

$\int T_R^* \, dv \geq 8$ K km s^{-1}, and the pedestal emission is most prominent the further one moves from position (0,2), which is situated adjacent to an integrated emission peak (see Fig. 6).

The position-velocity plots for both the N/S axis and the E/W axis (Figs. 13*a* and 13*b*) confirm the existence of the blueshifted pedestal. In Figure 13*a* emission from the clump is especially noticeable in the N/S plot at positions 0′ to 2′N. Although the blueshifted pedestal is present at this position, it becomes more prominent at positions 1′S and 3′ and 4′N. However, the spectrum at (0,4) indicates that another clump may be situated north of the mapped region.

The CO(2–1) high-sensitivity spectra were obtained at various locations in the mapped region, and they are shown individually in Figure 14. The positions of the CO(2–1) spectra are referred to the same (0,0) position as the CO(1–0) spectra. Two of the spectra, (8.2,29) and (10.7, −3) are outside the confines of the map shown in Figure 6. All of the five spectra within the mapped region show a blueshifted pedestal extending at least to -5.5 km s^{-1} and the spectra at positions (0,0), (3.2, −2.1), (−2.9,3.0), and (−1.4,1.5) show a redshifted pedestal extending to ~ 0.0 km s^{-1}. The line of sight at (−1.4, 1.5) is near a clump with $\int T_R^*[\mathrm{CO}(1\text{–}0)]\,dv \geq 8$ K km s^{-1}, and the pedestal in this spectrum is at a significantly higher antenna temperature than the pedestals at the other positions so that it begins to resemble a clump.

The spectrum at position (3.2, −2.1) is centered on the only *IRAS* point source within the mapped region. The *IRAS Point Source Catalog* (1985) lists for this position upper limits to the 12, 25, and 60 μm flux and a value of 2.31 Jy for the 100 μm flux. The 100 μm flux in the surrounding half degree is 18 MJy sr^{-1}, and the local cirrus is 5 times brighter than the source at 100 μm. The spectral signature for this source is drastically different from that of a typical embedded source (e.g., Beichman *et al.* 1986). It is almost certain that the *IRAS* point source at this position is due to cirrus contamination and is not due to any embedded young stellar object. A search for T Tauri stars in high-latitude molecular clouds was conducted by Magnani, Caillault, and Armus (1990) with negative results for the translucent clouds so that it is highly unlikely that any of the pedestals described in this paper are the result of star formation.

MBM 16.—The CO(1–0) channel maps in Figure 1 show one clearly defined clump in the 11′×8′ mapped region. However, data recently acquired from the FCRAO[5] 14 m telescope indicate that another clump exists near the western edge of the map. At the 1.5 K antenna temperature contour level, the central clump in the mapped region is 4′×7′ in extent which at 60–95 pc (Hobbs *et al.* 1988) corresponds approximately to 0.1 pc×0.2 pc. Ten high-sensitivity CO(1–0) spectra and four CO(2–1) spectra were obtained toward MBM 16 at the locations shown in Figure 4. The rms noise figures for these scans range from 0.06 to 0.17 K so that any emission with $T_R^* \sim 0.2-0.5$ K, depending on the scan, is unambiguously detected. Since there is only one prominent clump in the region, Gaussian fits to the spectra are thus more easily accomplished than for the other two regions. The Gaussian-fit parameters to the narrow-line emission for the CO(1–0) and CO(2–1) spectra are shown in Table 2, where the first column lists the position, the subsequent three columns list the Gaussian-fit parameters of antenna temperature, centroid velocity, and FWHM, and the last column presents the full velocity extent of all nonambiguous pedestal emission. The uncertainty in the Gaussian fits is typically less than 15%. In Figure 15 the CO(1–0) spectra are shown in the relative positions they occupy in Fig. 4 and the four individual CO(2–1) spectra are shown in Figure 16.

[5]The Five College Radio Astronomy Observatory is operated with permission of the Metropolitan District Commission and with support from the National Science Foundation.

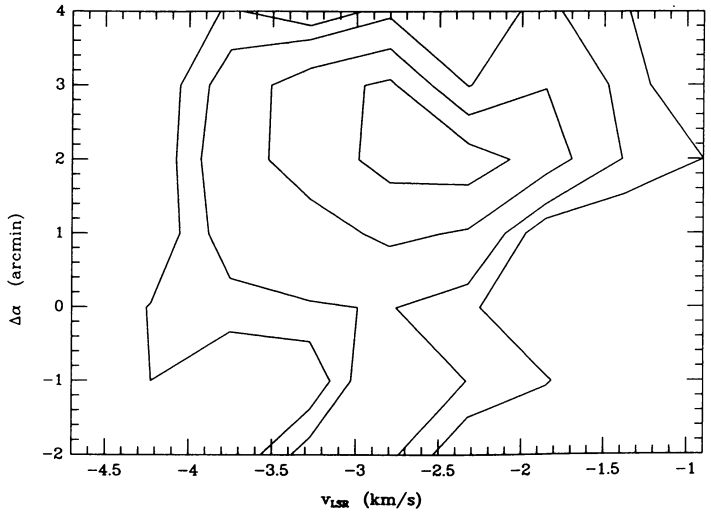

FIG. 10*a*

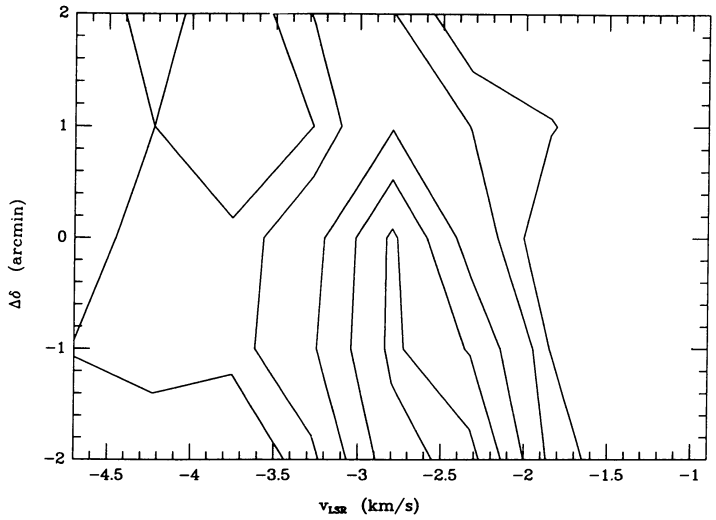

FIG. 10*b*

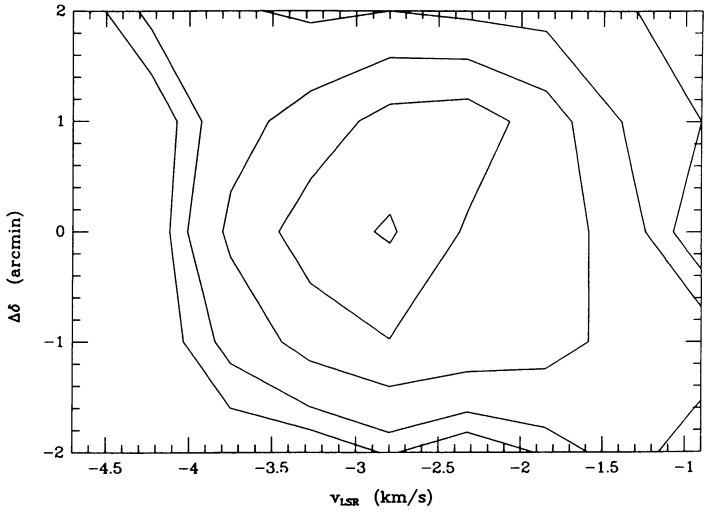

FIG. 10*c*

FIG. 10.—(*a*) Position-velocity plot for the region in MBM 32 in the E/W direction along the strip with right ascension 1′N of 66°05′00″. The positive offsets are east of $9^h25^m55^s$ at 1′ intervals and the negative offsets are west. The contour levels are at 0.4, 1, and 2 K and at succeeding 1 K intervals. The velocity resolution is 0.5 km s^{-1} and the spatial resolution is 1′. (*b*) Same as (*a*) but for a slice in the N/S direction along declination 1′W of $9^h25^m55^s$. Positive offsets are north of 66°05′ at and negative offsets are south. The region between $v = -3.5$ to -4.0 km s^{-1} and $\Delta\delta = 1'$–$2'$ is below the 0.4 K contour level. (*c*) Same as (*b*) but for a slice in the N/S direction along declination 2′E of $9^h25^m55^s$.

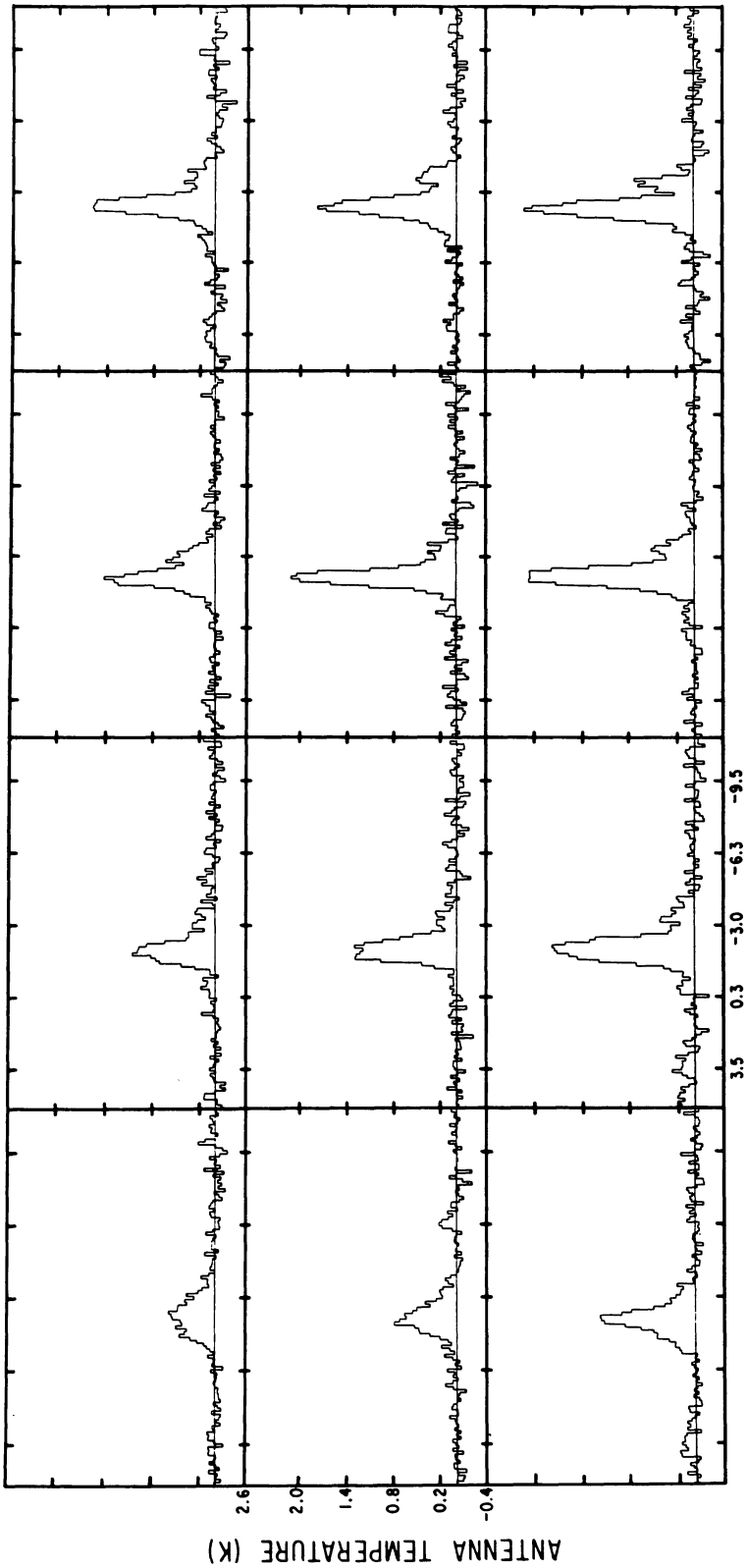

FIG. 11.—CO(2–1) high-sensitivity map at the positions in MBM 32 shown in Fig. 5. The (0, 0) position is defined to be the spectrum at the intersection of the labeled ordinate and abscissa and is located at $9^h25^m50^s$ and 66°05′30″. Note that for this map the velocity scale increases from right to left. The rms noise per channel ranges from 0.05 to 0.09 K, and the velocity resolution is 0.13 km s^{-1}. The spectra are one beamwidth (30″) apart, corresponding to 0.015 pc at the distance of the cloud.

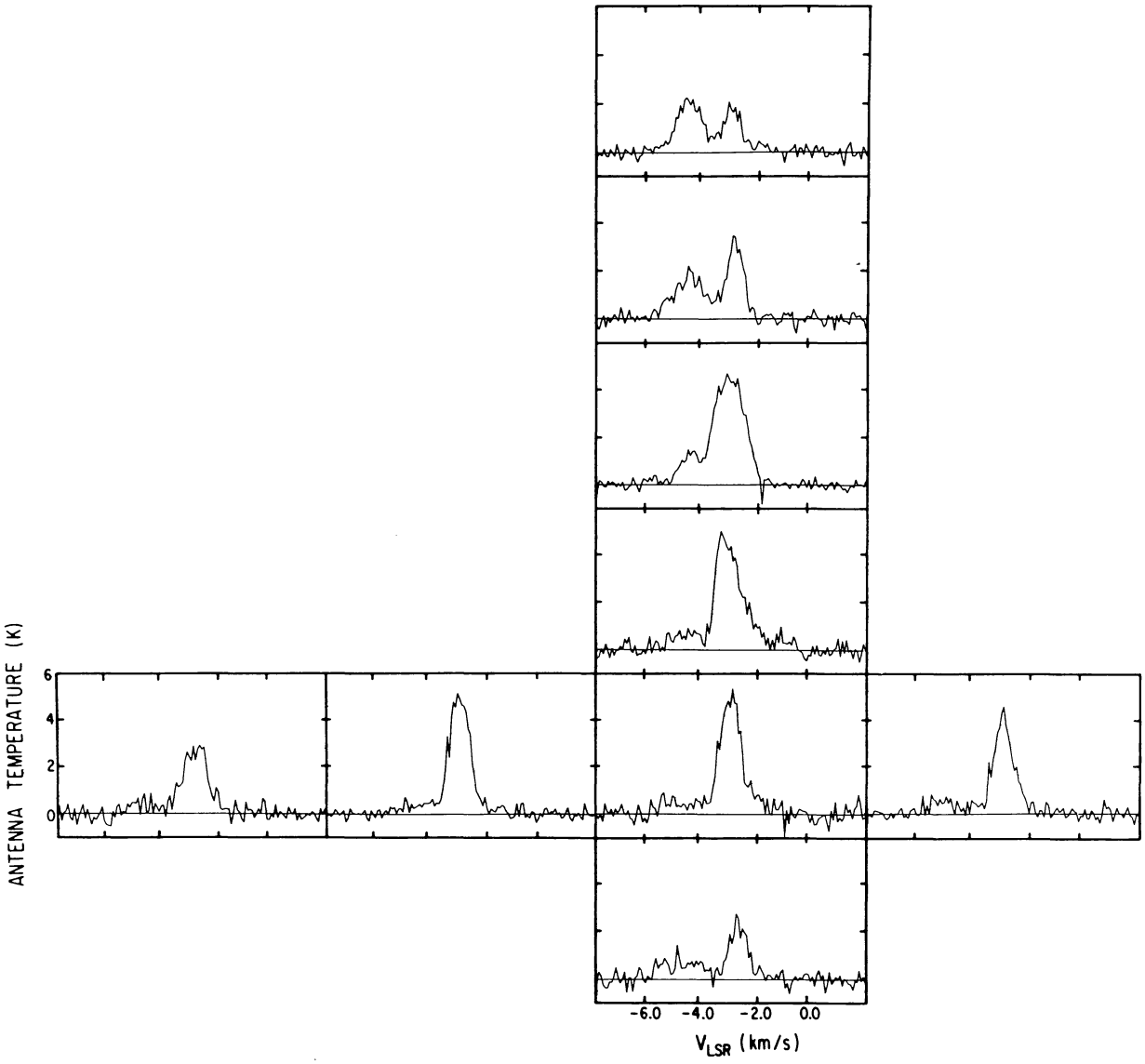

FIG. 12.—High-sensitivity CO(1–0) map at the positions in MBM 54 noted in Fig. 6. The rms noise per channel varies from 0.11 to 0.27 K and the velocity resolution is 0.08 km s^{-1}. The central position is at $23^h06^m48^s$ and 18°13′00″, and the spectra are separated by one beamwidth (1′).

The emission from the clump readily stands out in the central spectrum in Figure 15 and diminishes in intensity to the north, east, and west. Although the westernmost and easternmost CO(1–0) spectra show no sign of the narrow line emission, a CO(1–0) pedestal broader than the clump emission is clearly noticeable. This pedestal can be fitted with a Gaussian profile in both spectra (see Fig. 17), but the FWHM of the Gaussian is 2–3 times larger than the FWHM of the Gaussian profiles fit to the clump component present at the other positions (see Table 2). For the other spectra where the emission from the clump is most prominent, some trace of a blueshifted pedestal is discernible only at positions (0, −1), (0,0), (0,2), (−1,0), and perhaps (−2,0), while a redshifted pedestal is apparent only at positions (1,0) and (0,0).

Position-velocity plots along the two axes of the high-sensitivity maps are shown in Figure 18. Although the pedestal emission in the mapped region of MBM 16 is weaker than in the other two clouds, the position-velocity plot along the E/W axis (Fig. 18*a*) shows a blueshifted non-Gaussian component for the western scans. Similarly, the position-velocity plot along the N/S axis (Fig. 18*b*) shows a blueshifted non-Gaussian component for the southernmost scan and, perhaps, a redshifted wing for the northernmost scan.

The pedestal is much less noticeable in the CO(2–1) data presented in Figure 16. The spectra at positions (0,1) and (0, −1) show no trace of a pedestal although the blueshifted portion of the latter spectrum is contaminated by a bad off-position. Position (1,0) shows a definite blueshifted pedestal and possibly even a redshifted one. No spectra in the CO(2–1) transition are presently available for lines of sight away from the clump.

The salient feature of the pedestal emission in MBM 16 is that it becomes prominent only at the edges of the clump.

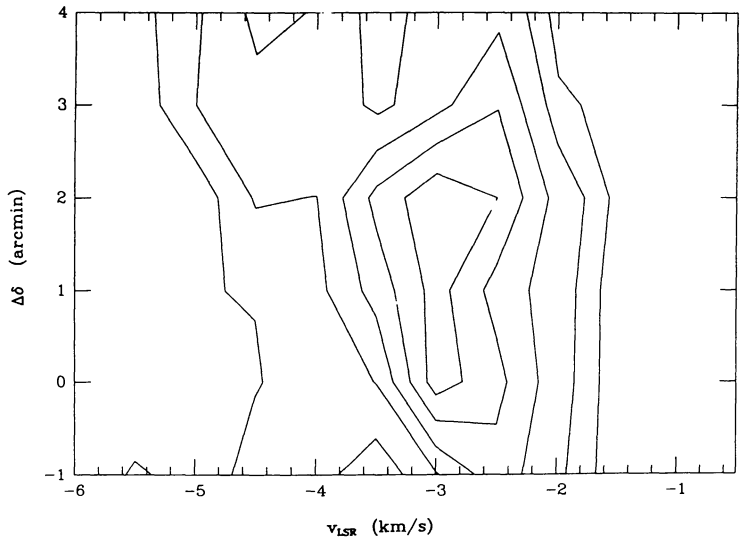

FIG. 13*a*

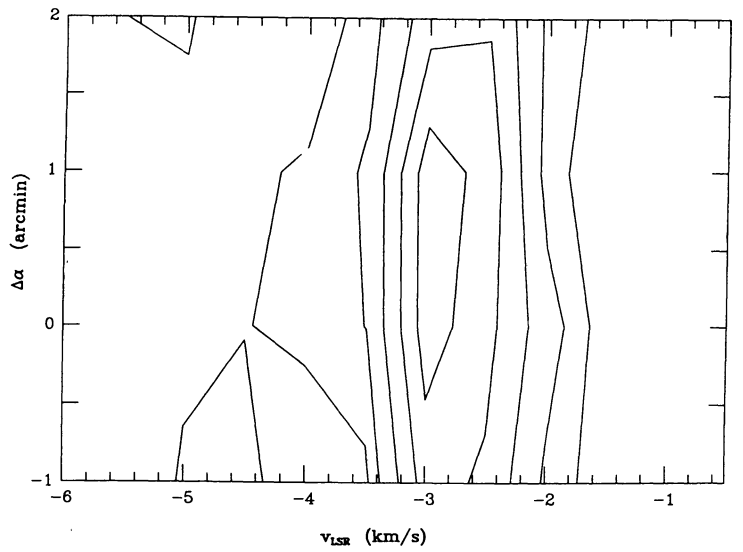

FIG. 13*b*

FIG. 13.—(*a*) Position-velocity plot for the region in MBM 54 in the N/S direction of the map shown in Fig. 12. The right ascension for this plot is $23^h06^m48^s$, and the *y*-axis shows the N/S offset in arcminutes from 18°13′00″. The contour levels are 0.4, 1, and 2 K and increase in 1 K intervals. (*b*) Same as (*a*) except that the slice is along the E/W axis of the map shown in Fig. 12. The declination for this plot is 18°13′00″, and the *y*-axis shows the E/W offset in arcminutes from $23^h06^m48^s$.

Although the pedestal is not as impressive as that in MBM 32 and MBM 54, the relevant scans for the region in MBM 16 are those away from the clump. Unfortunately, high-sensitivity spectra away from the clump at positions beside (3,0) and (−3,0) are not available at this time. However, the scans for the 11′×8′ region used to create the channel maps in Figure 1 are available, and when summed together they provide the necessary signal to noise to identify the pedestal emission. Figure 19*a* shows the summation of all the high-sensitivity spectra presented in Figure 15 and Figure 19*b* shows the summation of all the scans used to create the channel maps in Figure 1. Clearly, the pedestal is more evident in the summation of all the scans in the MBM 16 region and the emission extends from 6.0 to 10.0 km s^{-1}. Thus, in this particular cloud region, the pedestal appears to be a distributed component which is most prominent away from the main clump. However, more high-sensitivity mapping, especially to the west of this region, may reveal that the low-level emission arises from the outer portions of other nearby clumps. The parameters of the two Gaussians fitted to the profile in Figure 19*b* are listed in Table 2, and they indicate that the pedestal emission shares the same velocity centroid as the clump emission but is 4 times as wide.

In summary, for the regions in MBM 32 and 54, it appears that if a pedestal is present at a given velocity along a line of sight, then *in the vicinity* there will be a narrow-line compo-

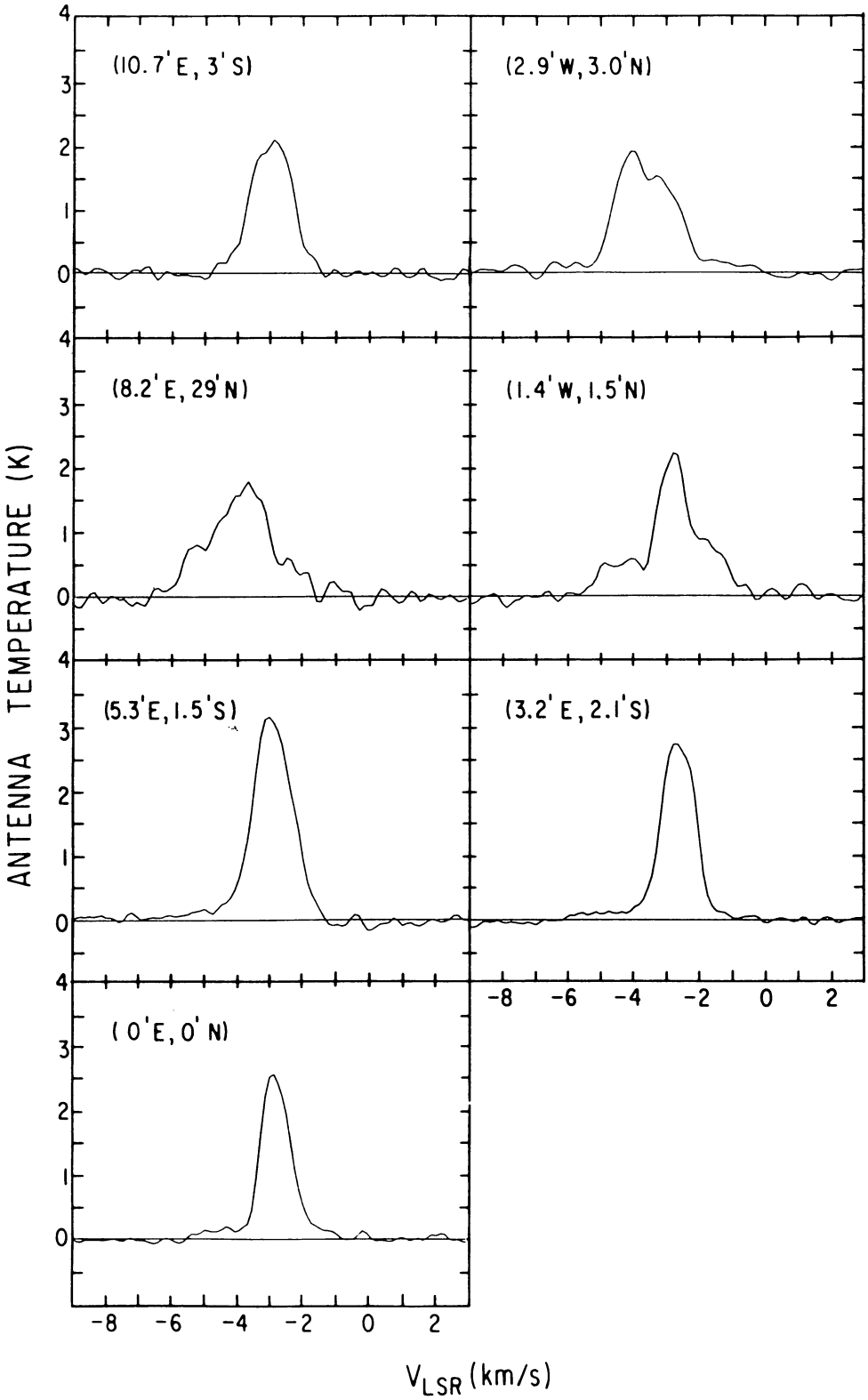

FIG. 14.—CO(2–1) high-sensitivity spectra at the positions in MBM 54 shown in Figure 6. The rms noise per channel is 0.05 to 0.11 K, and the velocity resolution is 0.13 km s^{-1}. The coordinates in the upper left corner of the spectra denote the position with respect to position (0,0) which is at $23^h06^m48^s$ and 18°13′00″.

TABLE 2

A. Gaussian-Fit Parameters for the Spectra in MBM 16

Position	T_R^*	V (LSR) (km s^{-1})	ΔV (core)[a] (km s^{-1})	ΔV (pedestal) (km s^{-1})
CO(J = 1–0) Beam: 1′				
3′W 0′N.....	0.32 K	7.61	2.05	6.1–9.0
2′W 0′N.....	2.35	8.08	0.70	6.8–9.0
1′W 0′N.....	7.04	7.95	0.77	6.9–9.0[b]
0′W 2′N.....	1.99	8.16	0.75	6.6–8.7
0′W 1′N.....	9.14	8.16	0.77	7.0–8.8
0′W 0′N.....	9.10	8.05	0.86	7.0–9.3
0′W 1′S	9.11	7.66	0.83	6.1–9.4
1′E 0′N	8.14	8.15	0.86	6.8–9.4
2′E 0′N	3.79	8.11	0.58	7.0–8.6
3′E 0′N	0.47	7.59	1.27	6.6–8.6
CO(J = 2–1) Beam: 30″				
0′W 1′N.....	5.34	7.85	0.88	6.6–9.0
0′W 0′N.....	5.15	7.91	0.96	6.0–8.9
0′W 1′S	5.08	8.10	0.89	7.1–9.2[c]
1′E 0′N	4.79	7.91	0.91	5.9–9.4

B. Sum of all CO(1–0) scans in Figure 1; Beam: 2′.3

T_R^*	V(LSR)	ΔV
0.98	7.87	0.76[d]
0.46	7.82	3.08

[a] Gaussian-fit FWHM.

[b] Contaminated off-position. The blueshifted emission probably extends to velocities < 6.9 km s^{-1}.

[c] Contaminated off-position. The blueshifted emission probably extends to velocities < 7.1 km s^{-1}.

[d] Two Gaussians fit to the data; Spectrum shown in Fig. 19*b*.

nent at the same velocity as the pedestal, but with a greater antenna temperature. For MBM 16 the situation differs because at a level of $T_A^* > 1.5$ K only one narrow-line component is present. Weak emission from the western edge of the map indicates that another clump is probably situated ~ 6′–8′ west of the main clump, but more data are required to verify this. Although some of the line profiles presented in this section resemble the wings associated with typical molecular outflows it is important to stress that the pedestal phenomenon in translucent high-latitude clouds is almost surely not associated with star formation.

IV. PHYSICAL PARAMETERS OF THE PEDESTALS AND CLUMPS

In order to understand the nature of the pedestal emission it is necessary to determine the gas density, temperature, and CO abundance of the pedestal with respect to the clump. In § IV*a* we determine the optical depth of the CO emission in the pedestals, and in § IV*b* we employ an LTE analysis to calculate the CO column density and abundance in the clump and the pedestal for one line of sight. The H_2 densities derived from an LVG approximation are discussed in § IV*c*. These calculations are restricted to position (0,0) in MBM 54, the only position with CO(1–0), CO(2–1), and ^{13}CO(1–0) data. Clearly, much more data, especially in the form of multitransition and isotopic studies, are required for a definitive explanation of the phenomenon. Due to the low antenna temperatures of the pedestals, further observations will require a large investment of telescope time.

a) CO *Opacity*

One of the first considerations in analyzing the CO data is to determine if the CO emission is optically thick. The Optical depth for the CO(1–0) transition is determined from the ^{12}CO/^{13}CO antenna temperature ratio and the assumption that the ^{12}CO/^{13}CO cosmic abundance is similar to the terrestrial abundance of 89 (e.g., Penzias 1980). Since the ^{12}CO/^{13}CO ratios for both the narrow and broad emission along the (0,0) line of sight of MBM 54 are less than 10, (BMW) the CO emission appears to be optically thick. There is additional evidence for optically thick pedestals: using the expression for the optically thin CO(2–1)/CO(1–0) line ratio as a function of excitation temperature, $4e^{-h\nu_{21}/kT_{ex}(2-1)}$ (Goldsmith, Plambeck, and Chiao 1975), and a typical T_{ex}(2–1) of 8–10 K (see below) yields a CO(2–1)/CO(1–0) line ratio of approximately unity. If the excitation temperature is greater than 10 K, then the CO(2–1)/CO(1–0) line ratio will be greater than one for optically thin emission. However, both for the clump and pedestal emission, *all* of the CO(2–1) spectra in the translucent clouds have substantially lower antenna temperatures than the CO(1–0) line. The CO(2–1)/CO(1–0) ratio is thus always significantly less than one implying that the CO emission in both the clumps and in the pedestals is optically thick (however, if the kinetic temperature is very low, ~ 3–5 K, then optically thin gas can give rise to CO(2–1)/CO(1–0) ratios below unity; see Levreault 1988).

In some cases, fractionation can decrease the ^{12}CO/^{13}CO ratio and thus cause optically thin gas to appear optically thick. We do not believe this is the situation in the translucent molecular clouds for the following reasons: Isotope selective photodissociation can increase the ^{12}CO/^{13}CO ratio counteracting some of the fractionation effect (Bally and Langer 1982; Chu and Watson 1983; Glassgold, Huggins, and Langer 1985). The ^{12}CO column density obtained with the LTE assumptions and the hydrogen column densities obtained from star counts for the translucent high-latitude clouds are consistent with ^{13}CO/H abundances typical of optically thick dark clouds (Magnani, Blitz, and Wouterloot 1988). In summation, the pedestal emission for the MBM 54 (0, 0) line of sight and other lines of sight with CO(2–1)/CO(1–0) ratios less than one is optically thick.

b) LTE *Analysis*

The excitation temperatures for the CO(1–0) and CO(2–1) transitions can be calculated under the LTE approximation assuming that the CO lines are optically thick. The CO and ^{13}CO spectra for the (0,0) line of sight in MBM 54 are presented in BMW. The excitation temperature can be obtained from

$$T_R(^{12}\mathrm{CO}) = \eta_f T_0 \left[f(T_{ex}) - f(T_{bg}) \right] \text{ (K)}, \qquad (1)$$

where T_{ex} is the excitation temperature, $T_0 = h\nu/k$, $f(T) = [e^{h\nu/kT} - 1]^{-1}$, T_R is the observed CO(1–0) antenna temper-

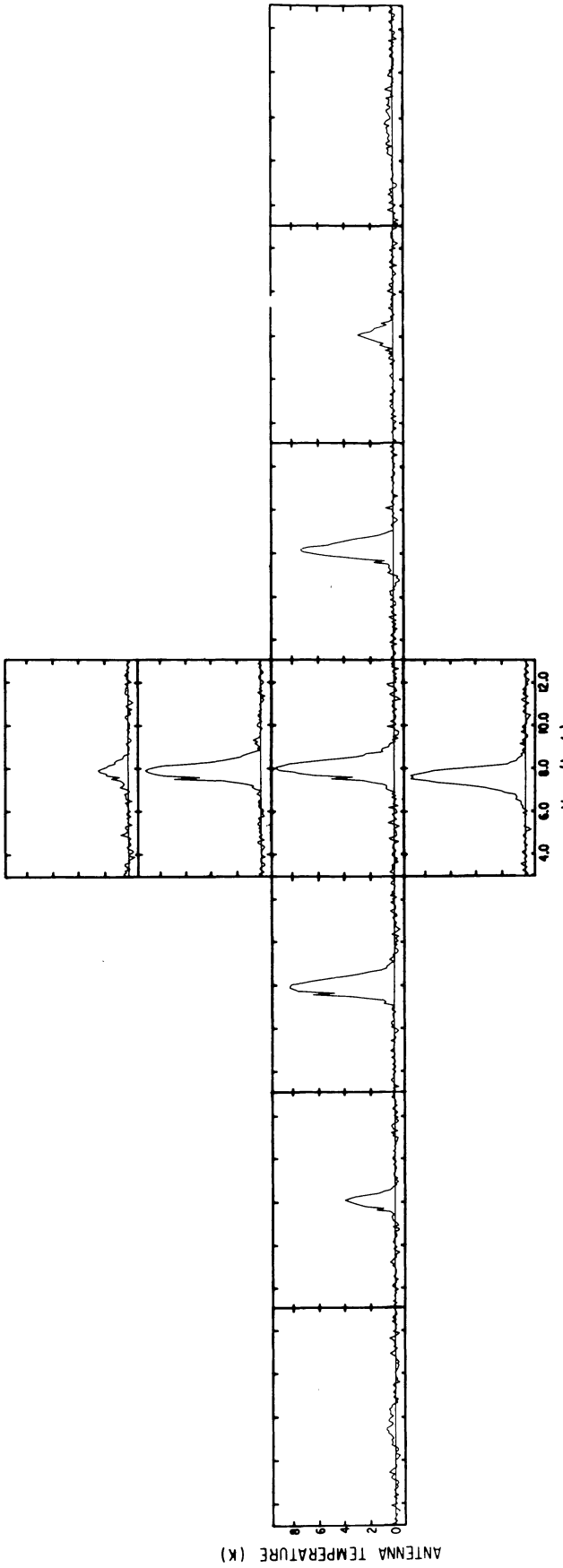

FIG. 15.—High-sensitivity CO(1–0) map at the positions in MBM 16 shown in Fig. 4. The rms noise level varies from 0.06 to 0.17 K, and the velocity resolution is 0.08 km s^{-1}. The dip visible in the spectra at $v \sim 7.6$ km s^{-1} is due to a bad channel. Gaussian-fit parameters for the narrow-line emission are presented in Table 2. The central scan [position (0, 0)] is at $3^h16^m20^s$, and 11°20′00″, and the spectra are separated by one beamwidth (1′).

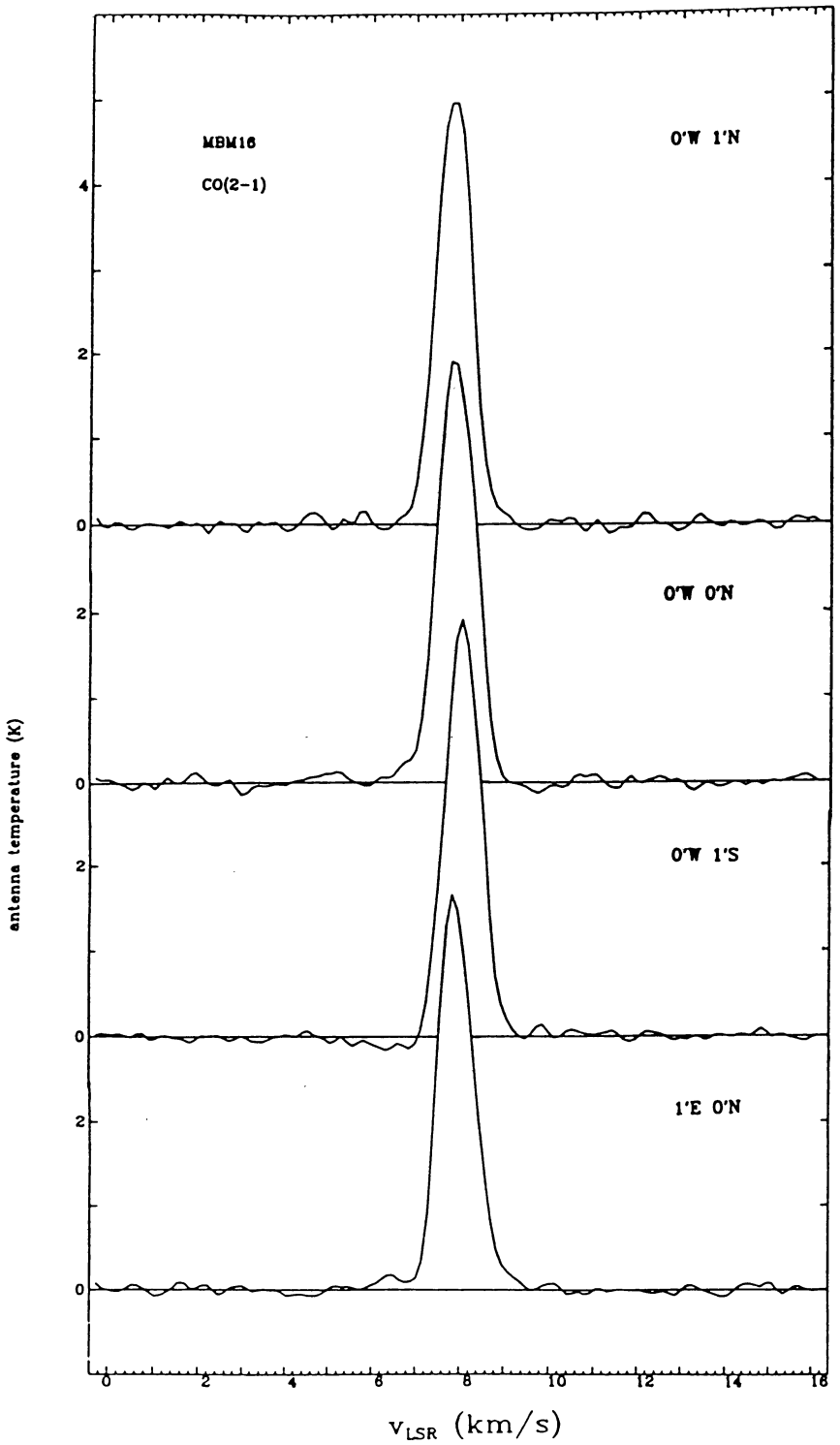

FIG. 16.—High-sensitivity CO(2–1) spectra at the positions in MBM 16 shown in Fig. 4. The rms noise per channel ranges from 0.03 to 0.05 K, and the velocity resolution is 0.26 km s^{-1}. The coordinates in the upper right corner of each spectrum are offsets in arcminutes from $3^h16^m20^s$, and 11°20′00″. Gaussian-fit parameters for the narrow-line emission are presented in Table 2.

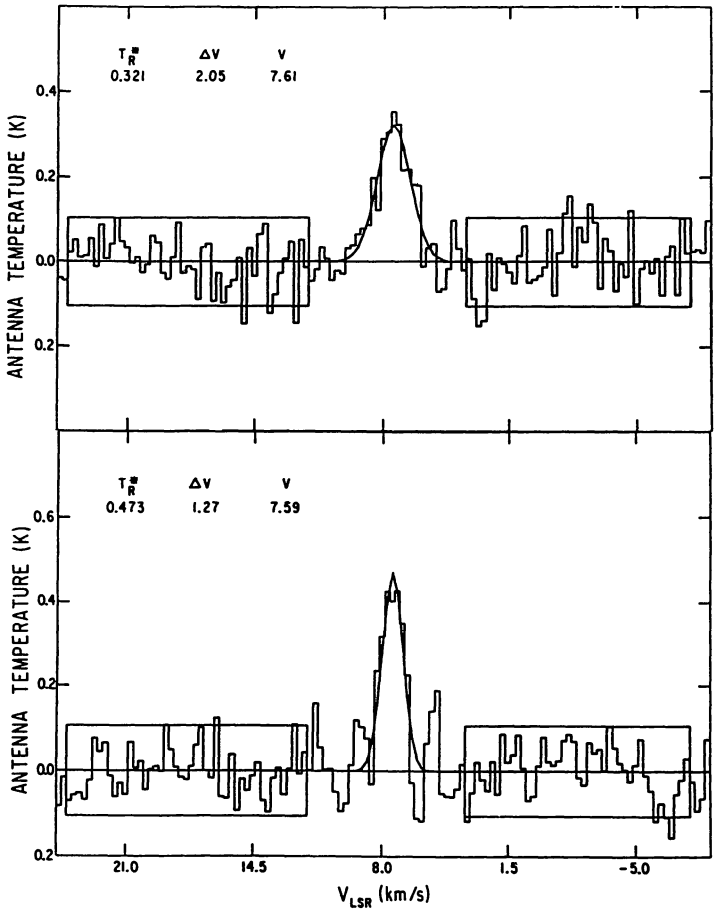

FIG. 17.—(*Top*) CO(1–0) spectra of the westernmost position in the MBM 16 high-sensitivity map (Fig. 15). The Gaussian fits to the spectrum are shown superposed on the data and the Gaussian parameters are presented in the upper left-hand corner. (*Bottom*) The easternmost position in the MBM 16 high-sensitivity map.

ature, T_{bg} is the background temperature equal to 2.7 K, and η_f is the area filling factor of the gas in the beam. If CO is thermalized, $T_{ex} = T_{kin}$, and T_{ex} is the same for all rotational levels. For several lines of sight in high-latitude molecular clouds for which CO(1–0) and CO(2–1) data are available, Magnani (1987) determined that in the range $4 \leq T_{ex} \leq 7$ K the data are consistent with thermalization. Assuming $\eta_f = 1$, the low antenna temperatures in the pedestals yield excitation temperatures of CO(1–0) and CO(2–1) derived from equation 1 of ~ 3 K. This in turn implies a kinetic temperature also of ~ 3 K; this value is clearly too low in light of the heating sources for molecular clouds of moderate to low extinctions (e.g., Hollenbach 1988). Thus the low derived kinetic temperature is most likely due to a value of η_f less than one; i.e., beam dilution of the pedestal region (see discussion in § V*b*). We assume in the following analysis that $T_{kin} = 10$ K for the (0,0) line of sight in MBM 54 for both the pedestal and clump emission, although it is conceivable that the kinetic temperature could be even higher in one or both regions.

The ^{13}CO LTE column density (N_{13}^*) is derived assuming $T_{ex}[^{13}\mathrm{CO}(1\text{–}0)] = T_{ex}[\mathrm{CO}(1\text{–}0)]$. However, for $n(\mathrm{H_2}) < 1000$ cm^{-3}, $T_{kin} = 10$ K, and $[^{12}\mathrm{CO}]/[^{13}\mathrm{CO}] = 60$, the assumption of equal excitation temperatures for the CO and ^{13}CO transitions does not hold; in fact, $T_{ex}[^{13}\mathrm{CO}(1\text{–}0)] < T_{ex}[\mathrm{CO}(1\text{–}0)]$, and the column density may be underestimated by a factor of 3 (Kutner and Leung 1985). Nevertheless, with the assumption of equal excitation temperatures, the ^{13}CO optical depth, τ^{13}, follows from:

$$T_R(^{13}\mathrm{CO}) = \eta_f T_0 \left[f(T_{ex}) - f(T_{bg}) \right] (1 - e^{-\tau^{13}}) \text{ (K)}. \quad (2)$$

Finally,

$$N_{13}^* = \left(2.4 \times 10^{14} T_{ex} \tau^{13} \Delta v\right) (1 - e^{-5.3/T_{ex}})^{-1} \text{ cm}^{-2}, \quad (3)$$

where Δv is the Gaussian-fit FWHM of the line in km s^{-1}. For the clump emission we derive $\tau^{13} \sim 0.2$; with a ^{13}CO FWHM = 0.7 km s^{-1} and $T_{ex} = 10$ K, then the MBM 54 (0,0) line of sight has $N_{13}^* = 8.2 \times 10^{14}$ cm^{-2}. If the depth of the clump is comparable to its linear size, the derived ^{13}CO column density is equivalent to a CO volume density of order 10^{-3} cm^{-3}. This value is similar to that obtained by Magnani (1987) using an LTE analysis on data for two clumps in MBM 16 and MBM 40.

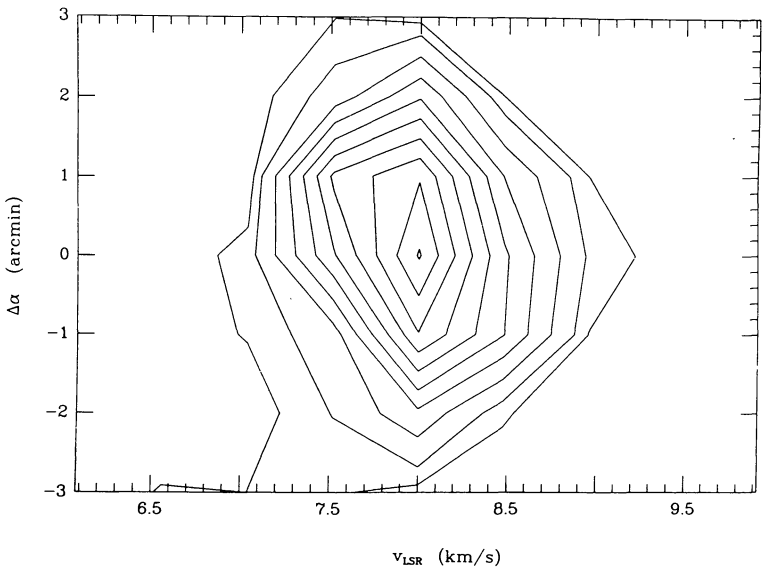

FIG. 18*a*

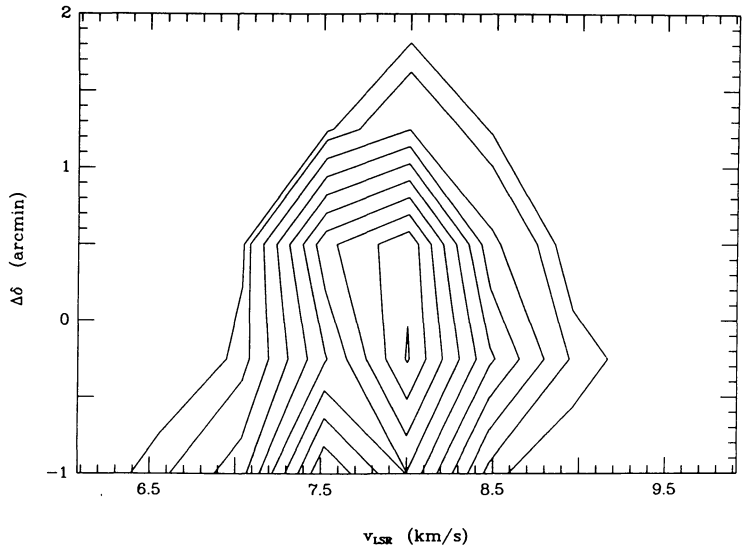

FIG. 18*b*

FIG. 18.—(*a*) Position-velocity plot along the E/W axis of the map shown in Fig. 15. The declination for this plot is 11°20′00″ and the *y*-axis shows the E/W offset from $3^h16^m20^s$ in arcminutes; east is positive and west is negative. The contour levels are set at 0.4, 1, and 2 K and at succeeding intervals of 1 K. The velocity resolution is 0.5 km s^{-1}, and the spatial resolution is 1′. (*b*) Same as Fig. 10*a* except that the slice is along the N/S axis of the map shown in Fig. 15. The right ascension for this map is $3^h16^m20^s$. The *Y*-axis shows the N/S offset in arcminutes from 11°20′00″; north is positive and south is negative.

An estimate of $N(H_{tot})$ can be obtained with the visual extinction and the Bohlin, Savage, and Drake (1978) $A_V - N(H_{tot})$ relationship for diffuse clouds. Unfortunately, extinction data for the region of MBM 54 are not available. We can estimate the extinction by using the average value for a sample of high-latitude clouds ($A_V \sim 0.6$ mag; Magnani and de Vries 1986). In this manner, $N(H_{tot})$ is of order 10^{21} cm^{-2} so that the ^{13}CO abundance is of order 10^{-6}, and the CO abundance is of order 10^{-4} in the clump.

For the pedestal, the calculation of the LTE ^{13}CO column density is much more difficult because η_f and T_{ex} are not known. Assuming $T_{ex} = 10$ K, and using values of $T_R(^{13}CO) = 0.04$ K and $\Delta v = 2$ km s^{-1} (BMW) in equation (2) gives a ^{13}CO optical depth of ~ 0.006 for a filling factor of 1. This implies that ^{12}CO is optically thin, in contradiction with the spectra presented in BMW for this particular line of sight. A filling factor of 0.1 for the pedestal gas yields a ^{13}CO optical depth of ~ 0.06, consistent with optically thick ^{12}CO emission. Equation (3) then gives $N_{13}^* \sim 7 \times 10^{14}$ cm^{-2}, so that even the pedestals have substantial CO column densities if $T_{ex} = 10$ K and $\eta_f = 0.1$. An increase in T_{ex} only increases the CO column density.

Since the column densities determined from LTE assumptions are similar in the two regimes, it is reasonable to

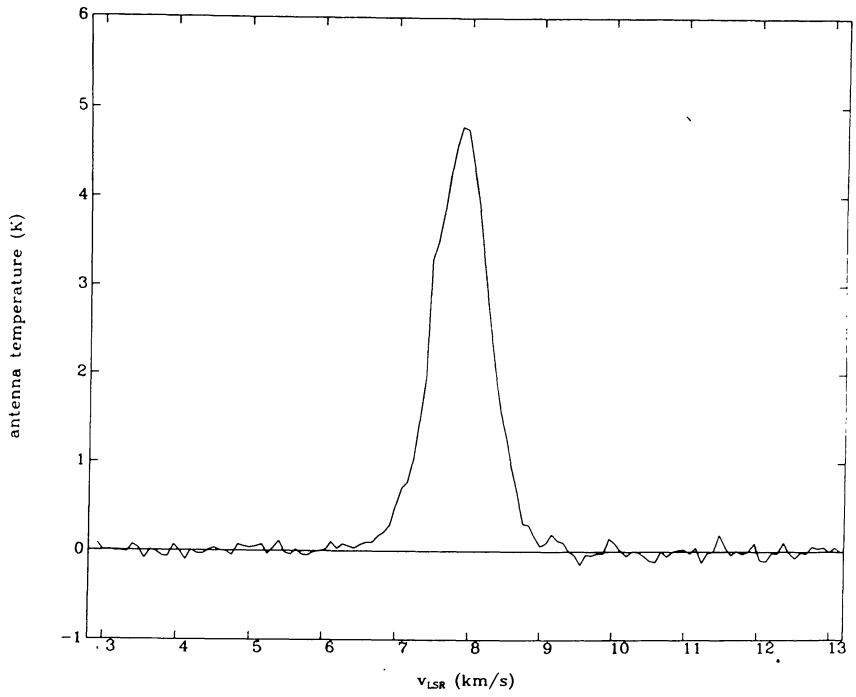

FIG. 19*a*

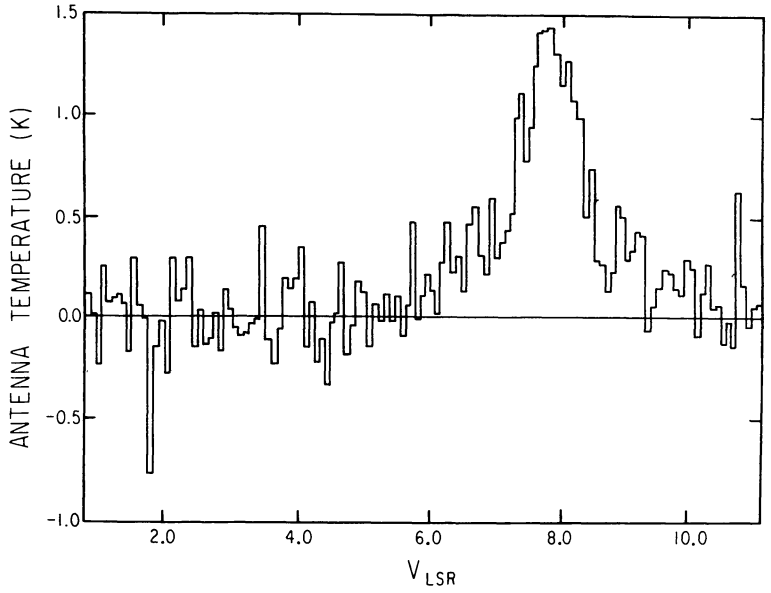

FIG. 19*b*

FIG. 19.—(*a*) Sum of all the CO(1–0) spectra in Fig. 15. The rms noise of the spectrum per channel is ~0.05 K, and the velocity resolution is 0.08 km s^{-1}. (*b*) Sum of all the CO(1–0) spectra used to produce the channel maps in Fig. 1. The rms noise of the spectrum is ~0.2 K per channel. Two Gaussians can be fitted to the data with the parameters shown in Table 2.

assume that the CO abundances are also similar. However, we cannot determine the volume densities of the gas without knowing the degree of clumpiness in the pedestal region and the overall spatial extent of the region. If the spatial extent of the pedestal is ~0.1 pc, the average density is a few times 10^3 cm^{-3}; and if the extent is ~1 pc, then the average density is a few times 10^2 cm^{-3}. In summary, for the (0,0) line of sight in MBM 54, the high-velocity dispersion gas responsible for the pedestal emission is *not* optically thin; the column density in the pedestal is not significantly different from that in the clump as long as the filling factor for the pedestal is substantially less than one and LTE assumptions are valid; and the density of the pedestal is of order 10^2 to 10^3 cm^{-3}.

c) *Large Velocity Gradient Analysis*

Goldsmith, Young, and Langer (1983) present $X(\mathrm{CO})/(dv/dr)$ versus $n(\mathrm{H_2})$ diagrams [the abundance, $X(\mathrm{CO})$, is defined as $n(\mathrm{CO})/n(\mathrm{H_2})$ and the units of the velocity gradient, dv/dr, are km $\mathrm{s^{-1}}$ $\mathrm{pc^{-1}}$] for analysis of the CO(1–0) and CO(2–1) lines using a large velocity gradient (LVG) radiative transfer model. Because their graphs conveniently display the CO(2–1)/CO(1–0) ratio and T_R(1–0), we will use them with the CO(2–1) and CO(1–0) profiles for position (0,0) in MBM 54 to determine the $\mathrm{H_2}$ densities in the clump and in the pedestal. For the clump, $T_R(1\text{–}0) \sim 4.8$ K and $T_R(2\text{–}1) \sim 2.6$ K; assuming a kinetic temperature of 10 K, the resulting value of $X(\mathrm{CO})/(dv/dr)$ is a few times 10^{-6} and the corresponding $n(\mathrm{H_2})$ is a few times 10^3 $\mathrm{cm^{-3}}$. This is in agreement with the LTE analysis of the clump in the preceding section and with the results for several core regions in the high-latitude clouds described by Magnani (1987). However, we note that recent studies by Heithausen, Mebold, and de Vries (1987) and Turner, Rickard, and Xu (1989) based on observations of $\mathrm{H_2CO}$ of the core regions of the high-latitude molecular clouds find significantly larger (10^4–10^5 $\mathrm{cm^{-3}}$) densities for the cores. This is not surprising because the CO(1–0) transition is not especially sensitive to gas with such densities.

The blueshifted region of the pedestal shows $T_R(1\text{–}0) \sim 0.4$ K and $T_R(2\text{–}1) \sim 0.1$ K. Although the beam sizes of our observations are different, we will assume, for the moment, that the gas filling factor is the same for both transitions. Using these values of the antenna temperature, and the same LVG model as above, we obtain values for $X(\mathrm{CO})/(dv/dr) \sim 5\times10^{-7}$ km $\mathrm{s^{-1}}$ $\mathrm{pc^{-1}}$ and a density $\sim 5\times10^2$ $\mathrm{cm^{-3}}$. If the filling factor is less than 0.2, then $X(\mathrm{CO})/(dv/dr) \geq 5\times10^{-5}$ km $\mathrm{s^{-1}}$ $\mathrm{pc^{-1}}$ and $n(\mathrm{H_2}) \leq 100$ $\mathrm{cm^{-3}}$.

If the pedestal emission arises from the outer regions of a clump, the gas in the pedestal will be exposed to a stronger UV radiation field than the gas in the clump. The kinetic temperature of the gas in the pedestal may thus be greater than the clump kinetic temperature. For the observed values of T_R(1–0) and T_R(2–1), a greater kinetic temperature does not greatly affect the $n(\mathrm{H_2})$ obtained from the LVG models; the density of the pedestal remains of order 10^2 $\mathrm{cm^{-3}}$. Unless the region giving rise to the pedestal emission is at least an order of magnitude greater in spatial extent that the region giving rise to the clump emission, this result contradicts the conclusion from the previous section that the LTE column densities in the pedestal and clump are the same. However, if the filling factor for the two transitions is different, the $T_R(2\text{–}1)/T_R(1\text{–}0)$ ratio changes. Different values of the density and $X(\mathrm{CO})/(dv/dr)$ are then possible and, consequently, different $n(\mathrm{H_2})$ and abundances are derived.

Since both the LTE and LVG methods are fraught with uncertainties, optically thin mass tracers such as CS or $\mathrm{H_2CO}$ must be used to determine more firmly the densities in the two regimes. We also note that, the assumption of optical thickness for the CO rests, as of this writing, on just one ^{13}CO spectrum; if this conclusion is to apply to *all* the lines of sight which show traces of a pedestal, significantly more ^{13}CO data are required.

V. POSSIBLE MODELS FOR THE PEDESTAL PHENOMENON

The lack of more sensitive and extended data and the uncertainties in the analyses mentioned above make it difficult to arrive unequivocally at a model which uniquely explains the observations. In this section we discuss two models which can reproduce the observed line profiles. The first model is based on the ideas presented in a recent paper by Keto and Lattanzio (1989), and the second model attributes the clump and pedestal emission to a superposition of two or more clumps each with a rapidly decreasing filling factor for the unresolved substructures which comprise the outer regions of each clump.

a) *Clump Collisions and Optically Thin Gas*

After failing to reproduce the observed column densities in the pedestals with a simple conduction front model, BMW suggested that collisions between the clumps in a high-latitude cloud might be responsible for the broad wings seen in the CO profiles. The suggestion was motivated by the apparently small surface filling fraction over the face of the high-latitude clouds which suggested that whatever is causing the wings is acting locally and not over the entire cloud. Furthermore, it was found that the extent of the wings does not exceed the velocity range exhibited by the central velocities of the clumps, so that the dynamics of the clumps themselves could provide the necessary energy and momentum to power the flows.

Following a similar suggestion made independently by Lattanzio and Henriksen (1988), Keto and Lattanzio (1989) have made a detailed hydrodynamic model with radiative transfer of the collision between two low-mass clouds. They leave the impact parameter and viewing angle as free parameters and calculate the expected line profile as a function of position in the cloud. They are able to reproduce the spectra published in BMW to within the noise providing good evidence that cloud collisions may be indeed the source of the pedestal emission. Furthermore, the models have predictive value in terms of what would be expected from other positions within the boundaries of a cloud. These authors are currently examining the data presented in this paper to see whether there is detailed agreement between their models and the mapping data.

However, it is already possible to find qualitative agreement with one of their models (see their Fig. 7) and the maps presented in this paper. Notably, one can identify the cold cores of the colliding clouds offset from one another both spatially and in velocity, and the pedestal components also can appear, as is evident from their figure. Comparing their figure to our Figure 12 shows good qualitative agreement.

In spite of this good agreement, at least one thorny issue remains. The radiative transfer in the Keto and Lattanzio models are made to follow the optically thin ^{13}CO gas, whereas our observations are primarily of CO. The problem stems from the CO(2–1) observations and the one ^{13}CO spectrum for MBM 54 which indicates that the CO is optically thick. How can the optically thick CO and the optically thin ^{13}CO trace the same kinematics? This problem is now an old one in molecular line astronomy and is usually solved

by invoking optically thick regions small compared to the beam which are kinematically decoupled from one another. The difficulty in this case is that the size of the clumps necessary to explain the observed line strengths begins to get uncomfortably small. If the clumps, for example, are on a scale which is 1/10 the scale of the CO(2–1) beam, then they would have diameters of 0.003 pc or 600 AU, only an order of magnitude larger than the solar system! The masses of these clumps would be planetary or subplanetary. Furthermore, unpublished observations of several high-latitude clouds at 12″ resolution (E. Falgarone and L. Blitz), do not show any evidence for small structure.

A definitive test of whether the solution to the problem lies in ultra–small-scale clumping or in the details of the radiative transfer can come from high-sensitivity ^{13}CO observations of the pedestals and from CO aperture synthesis of the pedestals. The ^{13}CO observations can tell us if indeed the Keto and Lattanzio radiative transfer properly treats the present observations, and the aperture synthesis can tell us if there is any power in the spatial frequencies that are large compared to the beam size of these observations.

b) *Decreasing Filing Factor of Unresolved Structure*

An alternative to the Keto and Lattanzio model postulates a quiescent, dense core and a larger, more turbulent, outer region with a decreasing filling of unresolved clumps. This model is, of course, not new and has been discussed often from the theoretical and observational point of view (e.g., Elmegreen 1985; Leung 1985; and references therein). A recent paper by Falgarone (1989) independently proposes this very mechanism as a means of producing the wing emission in the high-latitude clouds.

The low ^{13}CO/^{12}CO ratio and the CO(2–1) spectrum for the (0,0) position in MBM 54 indicates that the CO pedestal *is* optically thick, at least for this line of sight, so that $T_{ex} \sim T_K$. With T_R^* of only 0.4 K, the gas producing the pedestal for this line of sight would then have a kinetic temperature of slightly more than 3 K; this is much too cold for even a dense cloud core, and certainly for the outer, less dense regions which are probably the source of the pedestal. Thus, T_R should be significantly greater than T_R^*, implying that η_f is less than 1. If we assume that the core and the envelope of a clump are composed of unresolved substructures then a drop in the surface filling fraction in the envelope of an order of magnitude will produce the observed antenna temperatures for the pedestals. The greater velocity dispersion of the pedestals compared to the cores can result from equipartition of energy considerations. This is analogous to what has been observed for dark globules where a drop in the gas density in the outer regions results in an increased velocity dispersion (Leung 1985). The beam-dilution argument for low-level wings is not new; in giant molecular clouds both Bally *et al.* (1987) and Blitz and Stark (1986) argue that the interclump gas that they observe is composed of small, beam-diluted structures and Margulis and Lada (1986) attribute the broad wings observed in their survey of L1624 to beam-diluted bipolar outflows. However, the broad wings in the case of bipolar outflows are created by gas which is pushed or dragged by the wind from the stellar object at the center of the outflow. In our case, the different systemic velocities for the clump and pedestal are produced by the superposition of clumps, with the pedestal due to beam dilution of the outer regions of one of the clumps, and the narrow Gaussian line arising from the central regions of the other clump. Ironically, we also consider the N/S sequence of spectra shown in Figure 12 as significant evidence for this interpretation.

Two recent articles address similar observations of pedestals or of a distributed low-density component. LGW mapped the $6' \times 6'$ region centered on the line of sight to ζ Ophiuchi in the CO(1–0) and CO(2–1) transitions. Their data closely resemble some of the high-sensitivity maps presented in this paper but LGW choose to interpret the pedestals in the ζ Oph cloud as being composed of several narrow velocity components. To some extent the difference between that interpretation and our interpretation of a superposition of cores with extended envelopes is semantic: we both agree that there is more than one clump along the line of sight. However, the values of $[X(\mathrm{CO})/(dv/dr)]$ for the narrow velocity components in LGW are an order of magnitude lower than what we obtain for the pedestals and the CO column densities and abundances are nearly two orders of magnitude smaller than our results. Consequently, LGW state that the millimeter lines they observe in ζ Oph are optically thin. Our detection of a ^{13}CO pedestal in MBM 54 (BMW) implies that the CO is optically thick and that it is unlikely that the CO abundance in the pedestal for at least this one line of sight is significantly less than in the main clump. The discrepancies in the two results are due in part to the higher kinetic temperatures chosen by LGW for their LVG analysis. These differences in the physical parameters may be due to the inherent dissimilarity between the diffuse cloud in front of ζ Oph and the translucent high-latitude molecular clouds. The former has a CO/H_2 abundance of 9.1×10^{-7} (Duley and Williams 1984) while the high-latitude clouds have much greater CO abundances and densities and are thus very different chemically. We note that the diffuse cloud in front of ζ Oph has peak CO(1–0) antenna temperatures barely greater than 1 K while some of the lines of sight in the high-latitude clouds show antenna temperatures of up to 10 K. Van Dishoeck and Black (1988) discuss more thoroughly the chemical differences between diffuse and translucent clouds.

Blitz and Stark (1986) report broad, high-velocity (5–20 km s^{-1}) wings over several regions in the Rosette Giant Molecular Cloud (RMC). The broad wings are evident in the sum of all the individual spectra over the cloud and along lines of sight where long integrations were made. The authors conclude that the gas represented by the wings is pervasive throughout the RMC, and they have identified this gas as an interclump component which is slowly leaking out of the cloud. As in the case of the pedestals, the CO wings are optically thick. Furthermore, the gas is probably highly clumped (the volume filling fraction may be as low as 10^{-3}), thus explaining how the CO may be excited despite the apparent low average density. Although there are similarities between the two pedestal phenomena, it is important to stress that the wings in the RMC extend over the entire

cloud, while for the high-latitude clouds the pedestals appear to be localized phenomena.

Finally, Norman and Silk (1980) discuss a clumpy cloud model with many small dense clumps immersed in a diffuse, warmer interclump medium. The subsequent clump collisions in the cloud are predicted to produce Gaussian profiles with emission wings. Although the source for the material and the kinetic energy of the clumps is T Tauri star winds, which are not applicable to the clouds discussed in this paper, it is conceivable that another source of turbulence could drive the clump collisions and, subsequently, produce the pedestals.

Clearly, all the preceding models need further work. The observations and analyses in this paper identify some of the gas parameters of the clump and pedestal regions, but for a full understanding of the phenomenon, models of the kinematic behavior of clumps in small clouds need to be undertaken. Since there is as yet no consensus for even the clump mass spectrum in small clouds (e.g., Falgarone and Pérault 1987), a quantitative exposition of the pedestal phenomenon is presently unfeasible. Extensive observations are needed to identify the regions in a cloud which contain a pedestal and those which do not, to establish how many clumps there are per cloud or per cloud region, and to determine the composition of a clump especially as regards the radial density structure. With this empirical information, simulations of clumpy clouds for varying clump size distributions and kinematics in the manner of Keto and Lattanzio (1989) may then elucidate the physical mechanisms involved in producing the pedestal emission.

We thank Tom Armstrong for comments on an early version of the manuscript, and Elizabeth Lada for help with some of the figures. Part of this work was accomplished while J. M. C. was an undergraduate summer intern at the Arecibo Observatory under a program sponsored by the NSF.

REFERENCES

Armstrong, J. T., and Winnewisser, G. 1989, *Astr. Ap.*, **210**, 373.
Bally, J., and Langer, W. D. 1982, *Ap. J.*, **255**, 143.
Bally, J., Langer, W. D., Stark, A. A., and Wilson R. W. 1987, *Ap. J. (Letters)*, **312**, L45.
Beichman, C. A., Myers, P. C., Emerson, J. P., Harris, S., Mathieu, R., Benson, P. J., and Jennings, R. E. 1986, *Ap. J.*, **307**, 337.
Blitz, L., and Stark, A. A. 1986, *Ap. J. (Letters)*, **300**, L89.
Blitz, L., Magnani, L., and Wandel, A. 1988, *Ap. J. (Letters)*, **331**, L127 (BMW).
Bohlin, R. C. Savage, B. D., and Drake, J. F. 1978, *Ap. J.*, **224** 132.
Chu, Y.-H., and Watson, W. D. 1983, *Ap. J.*, **267**, 151.
Clark, F. O., Giguerre, P. T., and Crutcher, R. M. 1977, *Ap. J.*, **215**, 511.
Duley, W. W., and Williams, D. A. 1984, *Interstellar Chemistry*, (London: Academic).
Elmegreen, B. G. 1985, in *Protostars and Planets II*, ed. D. C. Black and M. S. Matthews (Tucson: University of Arizona Press), p. 33.
Evans, N. J., II, Kutner, M. L., and Mundy, L. G. 1987, *Ap. J.*, **323**, 145.
Falgarone, E. 1989, in *Structure and Dynamics of the Interstellar Medium*, ed. G. Tenorio-Tagle, M. Moles, and J. Melnick, (New York: Springer-Verlag), in press.
Falgarone, E., and Pérault, M. 1987, in *Physical Processes in Interstellar Clouds*, ed. G. E. Morfill and M. Scholer (Dordrecht: Reidel), p. 59.
_____. 1988, *Astr. Ap.*, **205**, L1.
Falgarone, E., and Puget, J. L. 1988, in *Galactic and Extragalactic Star Formation*, ed. R. E. Pudritz and M. Fich, (Dordrecht: Reidel), p. 195.
Frerking, M. A., and Langer, W. D. 1982, *Ap. J.*, **256**, 523.
Glassgold, A. E., Huggins, P. J., and Langer, W. D. 1985, *Ap. J.*, **290**, 615.
Goldsmith, P. F., Langer, W. D., and Wilson, R. W. 1986, *Ap. J. (Letters)*, **303**, L11.
Goldsmith, P. F., Plambeck, R. L., and Chiao, R. Y. 1975, *Ap. J. (Letters)*, **196**, L39.
Goldsmith, P. F., Young, J. S., and Langer, W. D. 1983, *Ap. J. Suppl.*, **51**, 203.
Heithausen, A., Mebold, U., and de Vries, H. W. 1987, *Astr. Ap.*, **179**, 263.
Heyer, M. H., Snell, R. L., Goldsmith, P. F., and Myers, P. C. 1987, *Ap. J.*, **321**, 370.
Hobbs, L. M., Blitz, L., Penprase, B. E., Magnani, L., and Welty, D. E. 1988, *Ap. J.*, **327**, 356.
Hollenbach, D. 1988, *Astr. Letters Comm.*, **26**, 191.
IRAS Point Source Catalog. 1985, Joint IRAS Science Working Group (Washington, DC: GPO).
Keto, E. R., and Lattanzio, J. C. 1989, *Ap. J.*, **346**, 184.
Knapp G. R., and Bowers, P. F. 1988, *Ap. J.*, **331**, 974.
Kutner, M. L., and Leung, C. M. 1985, *Ap. J.*, **291**, 188.
Kutner, M. L., and Ulich, B. L. 1981, *Ap. J.*, **250**, 341.
Lada, C. J. 1985, *Ann. Rev. Astr. Ap.*, **23**, 267.
Lada, E. A., and Blitz, L. 1988, *Ap. J. (Letters)*, **326**, L69.
Langer, W. D., Glassgold, A. E., and Wilson, R. W. 1987, *Ap. J.*, **322**, 450 (LGW).
Lattanzio, J. C., and Henriksen, R. N. 1988, *M.N.R.A.S.*, **235**, 565.
Leung, C. M. 1985, in *Protostars and Planets II*, ed. D. C. Black and M. S. Matthews (Tucson: University of Aronza Press), p. 104.
Levreault, R. M. 1988, *Ap. J. Suppl.*, **67**, 283.
Lichten, S. M. 1982, *Ap. J. (Letters)*, **255**, L119.
Magnani, L. 1987, Ph.D. thesis, University of Maryland.
Magnani, L., Blitz, L., and Mundy, L. 1985, *Ap. J.*, **295**, 402 (MBM).
Magnani, L., and de Vries, C. P. 1986, *Astr. Ap.*, **168**, 271.
Magnani, L., Blitz, L., and Wouterloot, J. G. A. 1988, *Ap. J.*, **326**, 909.
Magnani, L., Caillault, J.-P., and Armus, L. 1990, *Ap. J.*, in press.
Margulis, M., and Lada, C. J. 1986, *Ap. J.*, **309**, L87.
Myers, P. C., and Benson, P. J. 1983, *Ap. J.*, **266**, 309.
Norman, C., and Silk, J. 1980, *Ap. J.*, **238**, 174.
Penzias, A. A. 1980, *Science*, **208**, 663.
Pérault, M., Falgarone, E., and Puget, J. L. 1985, *Astr. Ap.*, **152**, 371.
Schneider, S., and Elmegreen, B. G. 1979, *Ap. J. Suppl.*, **41**, 87.
Schwartz, P. R., Gee, G., and Huang, Y.-L. 1988, *Ap. J.*, **327**, 350.
Turner, B. E., Rickard, L.-J, and Lan-Ping, Xu 1989, *Ap. J.*, **344**, 292.
van Dishoeck, E. F., and Black, J. H. 1987, in *Physical Processes in Interstellar Clouds*, ed. G. E. Morfill and M. Scholer (Dordrecht: Reidel), p. 241.
_____. 1988, *Ap. J.*, **334**, 771.

Leo Blitz and Biman B. Nath: Astronomy Program, University of Maryland, College Park, MD 20742

John M. Carpenter: Department of Physics and Astronomy, University of Massachusetts, Amherst, MA 01002

Namir E. Kassim: Center for Advanced Sensing, Naval Research Laboratory, Code 4030, Washington, DC 20375-5000

Loris Magnani: Arecibo Observatory, P.O. Box 995, Arecibo, PR 00613